RSC Advances

ROYAL SOCIETY OF CHEMISTRY

www.rsc.org/advances

View Article Online
DOI: 10.1039/C4RA01459F

DNA/protein binding and cytotoxicity studies of copper(II) complexes containing *N, N′, N″*-trisubstituted guanidine ligands

Kumaramangalam Jeyalakshmi,[a] Nagamani Selvakumaran,[a] Nattamai S. P. Bhuvanesh,[b] Anantharaman Sreekanth[a] and Ramasamy Karvembu[a*]

A series of *N, N′, N″*-trisubstituted guanidine ligands (L1-L5) and their copper(II) complexes (**1-5**) [Cu(II){$C_4H_3SCONC(NHR)NC_6H_5$}$_2$] [where R = *p*-tolyl (**1**), phenyl (**2**) benzyl (**3**), butyl (**4**) and cyclohexyl (**5**)] were synthesized and characterized by elemental analyses and UV-visible, FT-IR, ^{1}H & ^{13}C NMR / EPR and mass spectroscopic techniques. The molecular structure of L1-L5, **3**, and **5** was confirmed by single crystal X-ray crystallography. The single crystal X-ray structure of the complexes reveals the square planar geometry. The interaction of calf thymus DNA (CT-DNA) and bovine serum albumin (BSA) with the copper(II) complexes was investigated using UV-Visible and fluorescence spectrophotometric methods. Spectral evidences show intercalative mode of DNA binding (in the order of 10^4 M^{-1}) with the complexes. The Stern–Volmer quenching constant (K_q) values were found from competitive binding studies and found to be in the range of 1.07-1.30 × 10^5 M^{-1} for the complexes. Spectral evidences also show good binding property of the complexes with the protein. Complexes **3** and **4** showed significant cytotoxicity against human breast (MCF7) and lung cancer (A549) cell lines.

---

[a] *Department of Chemistry, National Institute of Technology, Tiruchirappalli - 620 015, India. E-mail address: kar@nitt.edu (R. Karvembu); Fax: +91 431 2500133; Tel: +91 431 2503631*

[b] *Department of Chemistry, Texas A & M University, College Station, TX 77842, USA*

Electronic supplementary information (ESI) available: Crystallographic data for the structures reported in this paper have been deposited with the Cambridge Crystallographic Data Centre (CCDC) as supplementary publication numbers (CCDC 984605, CCDC 984606, CCDC 984604, CCDC 984603, CCDC 984607, CCDC 984602, CCDC 984601 for L1, L2, L3, L4, L5, **3** and **5** respectively). Copies of the data can be obtained free of charge from the CCDC (12 Union Road, Cambridge CB2 1EZ, UK; Tel.: + 44-1223-336408; Fax: + 44-1223-336003; e-mail: deposit@ccdc.cam.ac.uk ; Web site http://www.ccdc.cam.ac.uk).

View Article Online
DOI: 10.1039/C4RA01459F

1. Introduction

There is a widespread interest in the identification and development of transition metal based compounds for biological applications. It is well known that DNA is an important cellular receptor. The interaction of metal complexes with DNA has recently gained much attention because it indicates that the complexes may have potential biological activity and their activity depends on the mode and affinity of the binding with DNA.[1–3] Even though many transition metal complexes were reported as antitumour agents and some of them were under clinical trials, developing copper-based metallodrug is of special importance because of its biocompatibility. Copper complexes have proved to be the best candidates towards the search of the metal complexes of biological importance.[4-6] Synthetic copper(II) complexes have been reported as potential anticancer and cancer inhibiting agents[7,8] and number of copper complexes[9,10] have been found to be active both *in vitro* and *in vivo*. Similarly, protein was also established as one of the main molecular targets in the action of anticancer agents.[11] The interaction between protein and drugs provides useful information on the structural features that determine the therapeutic effectiveness of drugs and also to study the pharmacological response of drugs.[12,13] Nowadays interaction of the proteins with the metal complexes become important in the search of new drug molecules.

The guanidine molecule, $(NH_2)_2C=NH$, is an important ingredient of both organic and inorganic chemistry. It is used to synthesize a number of biologically and pharmaceutically relevant compounds.[14-17] Guanidine derivatives are very useful pharmacophores in medicinal chemistry due to their capacity to interact with functional groups present in enzymes or receptors through hydrogen bonds and electrostatic interactions. The guanidine group also act as a inhibitor of urokinase which plays a vital role in tumor metastasis which implicated in a large number of malignancies, including breast, lungs, bladder, stomach, cervix, kidney, and brain cancers.[18,19] Various guanidine compounds have been synthesized and tested for their antitumor activity.[20,21] Copper complexes containing guanidine ligands are also found to have many biological applications.[22] For instance, copper(II) complexes of *bis*(2-pyridylmethyl)amine ligand with guanidinium pendant groups had an enhanced ability to cleave plasmid DNA and it can also act as RNA mimic.[23] Copper(II) complexes with guanidine ligands have been recently reported as urease inhibitors.[24] These stem a great interest to develop guanidine based copper(II) complexes for biological applications. Herein we report the synthesis and characterization of copper(II) complexes containing trisubstituted guanidine ligands. The interaction of the copper(II) complexes with CT-DNA and BSA was

View Article Online
DOI: 10.1039/C4RA01459F

studied using spectrometric methods. We have also tested the *in vitro* cytotoxicity of the copper(II) complexes against MCF7 and A549 cancer cell lines.

2. Results and discussion

2.1. Synthesis

The guanidine ligands (L1–L5) were synthesized by a mercury-promoted guanylation reaction from *N*-thiophenecarbonyl-*N*′-phenylthiourea (Scheme 1). The copper(II) complexes were synthesized using $Cu(CH_3COO)_2 \cdot H_2O$ as the precursor (Scheme 2). All the ligands and their copper(II) complexes were characterized by elemental analyses and/or various spectroscopic techniques. The molecular structure of L1-L5, **3** and **5** were confirmed by single crystal X-ray diffraction studies.

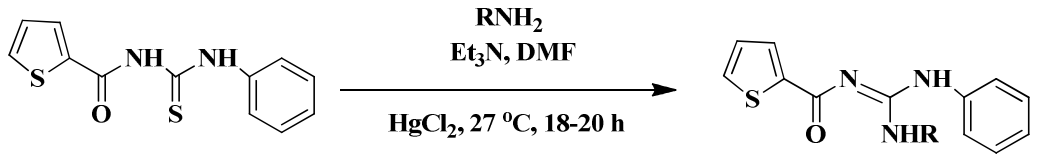

R= $C_6H_4CH_3$ (L1), C_6H_5 (L2), $CH_2C_6H_5$ (L3), n-C_4H_9 (L4) or C_6H_{11} (L5)

Scheme 1 Synthesis of *N*-phenyl -*N*′-(aryl/alkyl)-*N*″-thiophenecarbonylguanidine

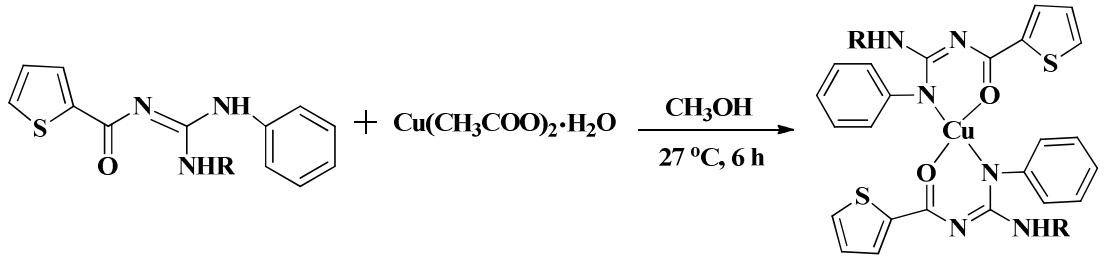

R= $C_6H_4CH_3$ (1), C_6H_5 (2), $CH_2C_6H_5$ (3), n-C_4H_9 (4) or C_6H_{11} (5)

Scheme 2 Synthesis of copper(II) complexes

2.2. Spectroscopy

The electronic spectra of the ligands showed two bands around 260 and 300 nm, which correspond to π-π^* and n-π^* transitions respectively. The spectra of the complexes exhibited three bands. Two bands appeared around 254-306 nm, which correspond to

View Article Online
DOI: 10.1039/C4RA01459F

intraligand transitions. The broad band in the region 601-626 nm corresponds to d-d transition.

In the FT-IR spectra of the ligands, two bands (strong and weak) were observed for N–H group in the range of 3367-3150 cm^{-1}. The weak band is due to the hydrogen bonded N–H. The C=N stretching frequency of the ligands was observed at 1588-1568 cm^{-1}. This is an intermediate value between double and single bonds, which shows the resonance between all the three nitrogen atoms in the guanidine moiety. The C=O stretching frequency appeared around 1632-1608 cm^{-1} in the spectra of the ligands was shifted to a lower value in the complexes, showing a single bond behaviour due to bonding with the Cu(II) ion. Further, the weak N–H band was disappeared, which indicates the coordination of N atom after deprotonation. The strong N–H band was appeared in the spectra of the complexes with minor shift towards higher value.

In the ^{1}H NMR spectra of the ligands (L1 and L2), signals of both the N–H protons were found in the same region (10.09-11.00 ppm) since both the N–H are attached to an aromatic ring. However, in the case of ligands L3, L4 and L5, one of the N–H protons gave signal in the up field range (4.40-5.25 ppm) and another in the down field range (11.82-11.69 ppm). Chemical shift of all other aromatic and aliphatic protons was observed in the expected regions. ^{13}C NMR spectra of the ligands showed resonance due to **C**=O and **C**=N in the regions 171.8-173.4 and 156.4–158.3 ppm respectively.[25]

X-band EPR spectra of the Cu(II) complexes were recorded at room temperature as well as at liquid nitrogen temperature in solid and solution states. The observation of quartet hyperfine structure on the parallel component is due to the interaction of unpaired electron of Cu(II) with Cu having nuclear spin I = 3/2.[26,27] All the complexes showed well resolved quartet hyperfine splitting typical of square planar Cu(II) system (Fig. 1), which was confirmed by single crystal XRD technique. For all the complexes $g_{\|} > g\square$ suggesting that the system is axial. The trend in the g value ($g_{\|} > g\square > 2.00$) and the value of exchange interaction term ($G > 4.0$) suggested that the unpaired electron of Cu(II) ion is present in the $dx^2–y^2$ orbital (Table 1).

2.3. Single crystal X-ray crystallographic studies

Thermal ellipsoid plots of ligands (L1-L5) and complexes (**3** and **5**) with the atomic labelling schemes are shown in the Figs. 2-8. Crystal data and selected inter atomic bond

View Article Online
DOI: 10.1039/C4RA01459F

lengths and angles are given in the Tables 2-5. The crystal structures of the ligands showed the existence of an intra molecular hydrogen bond between N–H and carbonyl oxygen. The thiophene ring was oriented in two opposite directions in the structures of L3-L5. Slightly elongated thermal parameters of the thiophene groups (S1, C1-C4) indicated a possible disorder, which was successfully modelled with a ratio of 90:10. The –C(O)N=C(NH–)(NH–) core exhibited a large amount of delocalization due to the Y-aromaticity, as can be observed by the C–N bond lengths [1.334-1.355 Å (L1), 1.332-1.353 Å (L2), 1.333-1.351 Å (L3), 1.329-1.350 Å (L4) and 1.329-1.356 Å (L5)].

Structures of **3** and **5** confirmed the square planar geometry of the complexes. Complex **3** crystallized in triclinic *P*-1 space group with *Z* of 1 and complex **5** crystallized in monoclinic *C*2/*c* space group with *Z* of 4. The Cu–N bonds are longer than the Cu–O bonds [Cu(1)–O(1) 1.9087 Å, Cu(1)–N(1) 1.9589 Å (**3**) and Cu(1)–O(1) 1.9069 Å Cu(1)–N(1) 1.9688 Å (**5**)], which are in the expected range for guanidine complexes.[28-31] Two guanidine ligands are coordinated to Cu(II) ion in a *trans* fashion. There is an increase in the C–O bond length and decrease in the C–N bond (involved in coordination) length in **3** and **5** compared to L3 and L5, respectively.

2.4. DNA binding studies

2.4.1. Electronic absorption titration

The Cu(II) complexes (**1-5**) showed absorption band at 291-298 nm, which was assigned to π-π^* transition. Upon the incremental addition of CT DNA to the complexes, the intensity of absorption decreases resulting in hypochromism ($\Delta\varepsilon$, 15-28%) with a small red shift. Intercalative mode of binding due to the strong stacking interaction between an aromatic chromophore and the base pairs of DNA usually results in hypochromism along with or without a small red or blue shift.[32] The extent of shift and hypochromism are normally found to correlate with the intercalative binding strength. The magnitude of hypochromism is in the order of **5**>**3**>**2**>**1**>**4**, which reflects the DNA binding affinities of the complexes. The absorption spectra of the complexes (**1-5**) in the presence and absence of CT DNA are shown in Fig. 9.

The binding constant of the complexes with CT DNA (K_b) was obtained from the ratio of slope to intercept in plots [DNA]/($\varepsilon_a - \varepsilon_f$) *versus* [DNA] according to the equation[33]

$$[DNA]/(\varepsilon_a-\varepsilon_f) = [DNA]/(\varepsilon_b-\varepsilon_f) + 1/K_b\,(\varepsilon_b-\varepsilon_f)$$

View Article Online
DOI: 10.1039/C4RA01459F

where [DNA] is the concentration of DNA in base pairs, ε_a is the apparent extinction coefficient value found by calculating A(observed)/[complex], ε_f is the extinction coefficient for the free compound, and ε_b is the extinction coefficient for the compound in the fully bound form. Each set of data, when fitted into the above equation, gave a straight line with a slope of $1/(\varepsilon_b - \varepsilon_f)$ and an y-intercept of $1/K_b(\varepsilon_b - \varepsilon_f)$ and the value of K_b was determined from the ratio of slope to intercept (Fig. 11). The magnitudes of intrinsic binding constants (K_b) are given in Table 6. The observed values of K_b revealed that the Cu(II) complexes bind to DNA *via* intercalative mode.[34] The K_b values were found to be in the range of 1.20-2.41 × 10^4 M^{-1}. Complex **5** showed better DNA binding affinity compared to the other complexes. The K_b value of **1**, **2**, **3** and **4** differs only by a small value. In complex **5**, the cyclohexyl ring is in the molecular plane, which might be the reason for its enhanced DNA binding ability compared to other complexes (**1-4**).

2.4.2. Fluorescence spectroscopic studies

Fluorescence property has not been observed for the complexes at room temperature in solution or in the presence of CT DNA. So the binding of the complexes with DNA could not be directly predicted through the emission spectra. Hence, competitive binding study was done to understand the mode of DNA interaction with the complexes.[35-37] Ethidium bromide (EB) emits intense fluorescence in the presence of CT DNA because of strong intercalation of the planar EB phenanthridine ring between adjacent base pairs in the double helix; therefore, EB has been considered as a typical indicator of intercalation.[38] If another molecule which can bind to DNA more strongly than EB was added, the molecule will replace the bound EB and there was a quenching in the DNA induced EB emission. The extent of quenching of CT DNA-EB reflects the extent of interaction with the added molecule. On adding Cu(II) complexes (0-25 μM) to CT DNA-EB, the quenching in the emission of DNA bound EB takes place (Fig. 10). Fluorescence quenching is explained by the Stern-Volmer equation[39]

$$F^o/F = 1 + K_q\,[Q]$$

where F^o and F are the fluorescence intensities in the absence and presence of complex respectively, K_q is a linear Stern-Volmer quenching constant, and [Q] is the concentration of complex. The slope of the plot of F^o/F *versus* [Q] gave K_q (Fig. 12). The apparent DNA binding constant (K_{app}) values were calculated by using the equation

$$K_{EB}\,[EB] = K_{app}\,[complex]$$

View Article Online
DOI: 10.1039/C4RA01459F

where [complex] is the complex concentration at 50% reduction in the fluorescence intensity of EB, $K_{EB} = 1.0 \times 10^7$ M^{-1} and [EB] = 5 μM. The quenching constant K_q and K_{app} values are listed in Table 6.

2.5 Protein binding studies

2.5.1. Absorbance and fluorescence studies

Fig. 13 shows the fluorescence emission spectra of BSA after the addition of complexes (**1**-**5**). When increasing amount of complex solution was added to a fixed quantity of BSA, there observed a decrease in the fluorescence intensity of BSA at 345 nm, upto 86.2, 88.5, 78.3, 74.6 and 83.5% for complexes **1**-**5** respectively, with bathochromic shift of 4, 3 and 1 nm for complexes **1**, **2** and **3** respectively. There was no appreciable shift in the case of complexes **4** and **5**. The observed hypochromicity has revealed that the complexes interact hydrophobically with the BSA protein.[40]

UV-Visible absorption titration of BSA with complexes (**1**-**5**) was done to predict the type of quenching process. Addition of the complex to BSA lead to an increase in BSA absorption intensity without affecting the position of absorption band. This indicates that the type of interaction between Cu(II) complexes and BSA was mainly a static quenching process.[41] The representative absorption titration spectrum is shown in Fig. 14. The fluorescence quenching is described by the Stern-Volmer relation

$$F^o/F = 1 + K_q\,[Q]$$

where F^o and F demonstrate the fluorescence intensities in the absence and presence of quencher, respectively. K_q is a linear Stern-Volmer quenching constant, and [Q] is the quencher concentration. The quenching constant (K_q) can be calculated using the plot of log (F^o/F) *versus* log [Q] (Fig. 15). When small molecules bind independently to a set of equivalent site, on a macromolecule, the equilibrium between free and bound molecules is represented by the Scatchard equation[42, 43]

$$\log[(F^o - F)/F] = \log K_b + n \log[Q]$$

where K_b is the binding constant of the complex with BSA and n is the number of binding sites. From the plot of log[(F^o–F)/F] *versus* log[Q] (Fig.16), the number of binding sites (n) and the binding constant (K_b) values have been obtained. The quenching constant (K_q), binding constant (K_b) and number of binding sites (n) for the interaction of the Cu(II) complexes with BSA are shown in Table 7. In all the complexes, only one binding site is available to interact with BSA. Results showed that complexes **1** and **2** interact strongly with BSA compared to **3**, **4** and **5**.

View Article Online
DOI: 10.1039/C4RA01459F

2.5.2 Characteristics of synchronous fluorescence spectra

Synchronous fluorescence spectroscopy provides information about the molecular microenvironment, particularly in the vicinity of the fluorophore functional groups.[44] Tyrosine, tryptophan and phenylalanine residues are responsible for the fluorescence property of BSA. The difference between the excitation and emission wavelength ($\Delta\lambda$) reflects the nature of the chromophore.[45] The large $\Delta\lambda$ value, such as 60 nm, is characteristic of tryptophan residue and a small $\Delta\lambda$ value, such as 15 nm, is characteristic of tyrosine. The synchronous fluorescence spectra of BSA with various concentrations of Cu(II) complexes (**1**-**5**) were recorded at $\Delta\lambda$ = 15 nm and $\Delta\lambda$ = 60 nm. On addition of the complexes, the fluorescence intensity of tryptophan residue at 340 nm decreased in the magnitude of 82.6, 88.9, 79.2, 71.0 and 80.3% for complexes **1**, **2**, **3**, **4** and **5** respectively (Fig. 17). Similarly, there was also decrease in the intensity of tyrosine residue at 300 nm. The magnitude of decrease was 86.6, 88.0, 80.0, 74.0 and 85.1% for complexes **1**-**5** respectively (Fig. 18). The synchronous fluorescence spectral studies clearly suggested that the fluorescence intensities of both the tryptophan and tyrosine were affected with increasing concentration of the complexes. The results indicate that the interaction of complexes with BSA affects the conformation of both tryptophan and tyrosine micro-region.[46]

2.6 Cytotoxicity assay

The cytotoxicity of the Cu(II) complexes (**1**-**5**) toward MCF7 (human breast cancer cells) and A549 (human lung cancer cells) cells has been examined by using MTT assay and compared with cyclophosphamide [IC_{50} = 6.58 μM (MCF7) and 22.36 μM (A549)] under identical conditions.[47] Figs. 19 and 20 show the cytotoxicity of the compounds (**1**-**5**) after 24 h incubation on MCF7 and A549 cancer cell lines, respectively. Complexes **3** and **4** exhibited cytotoxicity with IC_{50} values of 76.05 and 61.08 μM, respectively, against MCF7 cell line. The same complexes showed IC_{50} values of 91.68 and 68.8 μM against A549 cell line. Complexes **1** and **5** possess a moderate cytotoxicity. The IC_{50} values of **1** and **5** were found to be 128.67 and 145.0 μM, respectively, against MCF7. The same complexes showed IC_{50} values of 241.58 and 164.01 against A549. Complex **2** exhibited least activity than the other complexes. The IC_{50} values of all the complexes are listed in Table 8.

View Article Online
DOI: 10.1039/C4RA01459F

3. Conclusion

Five Cu(II) complexes with trisubstituted guanidine ligands have been synthesized. Single crystal X-ray diffraction studies revealed that the Cu(II) complexes have square planar geometry. The DNA binding of the complexes was investigated using absorption and fluorescence spectrometric techniques. The results supported the interaction of the complexes with CT DNA through non-covalent intercalation. The good protein binding ability of the complexes was revealed from fluorescence measurement. *In vitro* cytotoxicity results showed that the complexes have moderate activity against MCF7 and A549 cancer cell lines. The result of DNA binding does not correlate with that of the *in vitro* cytotoxic studies. This clearly states that the mechanism involved in cytotoxic activity of the complexes is different. Further studies are needed to study the relation between the DNA binding and cytotoxic activity of the complexes.

4. Experimental

4.1. Materials and methods

All the chemicals were purchased from Sigma Aldrich / Merck and used as received. Solvents were purified according to standard procedures. The melting points were determined on Lab India instrument and are uncorrected. The elemental analyses were performed using a Vario EL−III CHNS analyzer. FT-IR spectra were obtained as KBr pellets using a Nicolet-iS5 spectrophotometer. UV-Visible spectra were recorded using a Shimadzu-2600 spectrophotometer. Emission spectra were measured on a Jasco V-630 spectrophotometer using 5% DMF in buffer as the solvent. NMR spectra were recorded in $CDCl_3$ by using TMS as an internal standard on a Bruker 400 MHz spectrometer. EPR spectra were recorded on a JEOL EPR spectrometer at room temperature and liquid nitrogen temperature, operating at X-band frequency (9.1 GHz).

4.2. Synthesis of *N, N′, N″*-trisubstituted guanidines

The guanidine ligands were synthesized from *N*-thiophenecarbonyl-*N′*-phenylthiourea by a guanylation method.[48] The thiourea was mixed with the desired substituted amine in DMF in an equimolar ratio with two equivalents of triethylamine. The temperature was maintained below 5 °C using an ice bath and one equivalent of mercuric chloride was added to the reaction mixture with vigorous stirring. The ice bath was removed after 30 minutes, while the stirring continued overnight. The progress of the reaction was monitored using TLC

View Article Online
DOI: 10.1039/C4RA01459F

until all the thiourea was consumed. 20 mL of chloroform was added to the reaction mixture and the suspension was filtered through a sintered glass funnel to remove the HgS residue. The solvents were evaporated under reduced pressure and the solid residue was dissolved in 20 mL of CH_2Cl_2, then washed with water and the organic phase was dried over anhydrous Na_2SO_4. The residue obtained after evaporation of the solvent was recrystallized from ethanol to get crystals of the title compounds.

4.2.1. *N*-Phenyl -*N′*-(4-methylphenyl)-*N″*-thiophenecarbonylguanidine (L1)

Yield: 79%. Colourless solid. M.p.: 130 °C. UV−Vis (5% $CHCl_3$): λ_{max}, nm (ε, $dm^3mol^{-1}cm^{-1}$) 265 (23300), 301 (26900). FT-IR (KBR, ν cm^{-1}): 3279, 3203 (N–H), 1611 (C=O), 1568 (C=N). ^{1}H NMR (400 MHz, DMSO-d_6): δ, ppm 2.26 (s, 3H), 7.44-7.011 (m, 9H), 7.65 (d, *J* = 3.6 Hz, 1H,), 7.58 (d, *J* = 2.4 Hz, 1H), 7.08 (t, *J* = 3.6 Hz, 1H), 10.46 (s, 1H), 10.09 (s, 1H). ^{13}C NMR (100 MHz, DMSO-d_6): δ, ppm 21.0 (aliphatic CH_3), 123.9, 124.2, 125.1, 128.4, 129.9, 130.8, 132.1, 134.7. 135.1, 138.1, 144.4 (aromatic C), 156.4 (C=N), 171.8 (C=O). HRMS Calcd for $C_{19}H_{17}N_3OS$: 335.4228 Found: 335.4197.

4.2.2. *N,N′*-Diphenyl-*N″*-thiophenecarbonylguanidine (L2)

Yield: 78%. Colourless solid. M.p.: 120 °C. UV−Vis (5% $CHCl_3$): λ_{max}, nm (ε, $dm^3mol^{-1}cm^{-1}$) 266 (13500), 302 (16800). FT-IR (KBR): ν, cm^{-1} 3394, 3165 (N–H), 1602 (C=O), 1571 (C=N). ^{1}H NMR (400 MHz, $CDCl_3$) δ, ppm: 7.09 (t, *J* = 4 Hz, 1H), 7.07-7.46 (m, 11H), 7.79 (d, *J* = 3.6 Hz, 1H), 10.30 (s, 2H). ^{13}C NMR (100 MHz, $CDCl_3$): δ, ppm 124.1, 126.1, 127.7, 129.5, 130.9, 131.1, 136.3, 144.4 (aromatic C), 156.1 (C=N), 173.3 (C=O). HRMS Calcd for $C_{18}H_{15}N_3OS$: 321.3962 Found: 321.4001.

4.2.3. *N*-Phenyl -*N′*-benzyl-*N″*-thiophenecarbonylguanidine (L3)

Yield: 82%. Colourless solid. M.p.: 100 °C. $C_{19}H_{17}N_3OS$ (335.42). UV−Vis (5% $CHCl_3$): λ_{max}, nm (ε, $dm^3mol^{-1}cm^{-1}$) 262 (15000), 296 (28500). FT-IR (KBR): ν, cm^{-1} 3267, 3202 (N–H), 1611 (C=O), 1569 (C=N). ^{1}H NMR (400 MHz, $CDCl_3$): δ, ppm 4.72 (s, 2H), 5.25 (s, 1H), 7.07 (t, *J* = 3.6 Hz, 1H), 7.43-7.23 (m, 11H), 7.80 (d, *J* = 2.4 Hz, 1H), 11.82 (s, 1H,). ^{13}C NMR (100 MHz, $CDCl_3$): δ, ppm 45.2 (aliphatic, CH_2), 125.7, 127.2, 127.7, 127.8, 128.8, 130.2, 130.5, 130.7, 135.8, 144.8 (aromatic C), 158.2 (C=N), 173.4 (C=O). HRMS Calcd for $C_{19}H_{17}N_3OS$: 335.4228 Found: 335.4194.

View Article Online
DOI: 10.1039/C4RA01459F

4.2.4. *N*-Phenyl -*N′*-butyl-*N″*-thiophenecarbonylguanidine (L4)

Yield: 74%. Colourless solid. M.p.: 80 °C. $C_{16}H_{19}N_3OS$ (301.40). UV−Vis (5% $CHCl_3$): λ_{max}, nm (ε, $dm^3mol^{-1}cm^{-1}$) 264 (9400), 296 (24300). FT-IR (KBR): ν, cm^{-1} 3341, 3230 (N–H), 1607 (C=O), 1556 (C=N). ^{1}H NMR (400 MHz, $CDCl_3$): δ, ppm 0.92-0.95 (t, *J* = 5.6 Hz, 3H), 1.340-1.38 (q, *J* = 5.6 Hz, 2H), 1.564-1.550 (t, *J* = 5.6 Hz, 2H), 3.46 (s, 2H), 4.96 (s, 1H), 7.68-7.05 (m, 8H), 11.69 (s, 1H). ^{13}C NMR (100 MHz, $CDCl_3$): δ, ppm 13.9, 20.1, 31.9, 41.2 (aliphatic), 125.6, 127.1, 130.2, 130.3, 130.5, 135.9, 140.5 (aromatic C), 158.3 (C=N), 172.8 (C=O); HRMS Calcd for $C_{16}H_{19}N_3OS$: 301.4066 Found: 301.4001.

4.2.5. *N*-Phenyl -*N′*-cyclohexyl-*N″*-thiophenecarbonylguanidine (L5)

Yield: 71%. Colourless solid. M.p.: 131 °C. $C_{18}H_{21}N_3OS$ (327.44). UV−Vis (5% $CHCl_3$): λ_{max}, nm (ε, $dm^3mol^{-1}cm^{-1}$) 263 (7700), 296 (17300). FT-IR (KBR): ν, cm^{-1} 3307, 3207 (N–H), 1608 (C=O), 1553 (C=N). ^{1}H NMR (400 MHz, $CDCl_3$): δ, ppm 2.05-1.15 (m, 11H), 4.80 (s, 1H), 7.07 (t, *J* = 3.6 Hz, 1H), 7.41-7.23 (m, 6H), 7.77 (s, 1H), 11.71 (s, 1H). ^{13}C NMR (100 MHz, $CDCl_3$): δ, ppm 24.9, 25.6, 33.1, 50.4 (aliphatic C), 125.3, 126.8, 127.1, 127.7, 130.2, 136.1, 145.1 (aromatic C), 157.3 (C=N), 172.7 (C=O); HRMS Calcd for $C_{18}H2_1N_3OS$: 327.4438 Found: 327.4397.

4.3. Synthesis of copper(II) complexes (1-5)

The methanolic solution of $Cu(CH_3COO)_2{\cdot}H_2O$ (1 mmol) was added into the solution of an appropriate guanidine (2 mmol) in methanol at room temperature. The reaction mixture was stirred for 6 h under an inert atmosphere, and then the precipitate formed was filtered and washed with methanol. The suitable crystals of **3** and **5** for X-ray diffraction were grown from $CHCl_3$/n-hexane mixture (1:1).

4.3.1. Bis(*N*-phenyl-*N′*-(4-methylphenyl)-*N″*-thiophenecarbonylguanidinato)copper(II) (1)

Yield: 74%. Light blue solid. M.p.: 212 °C. Anal. Calcd. for $C_{38}H_{32}CuN_6O_2S_2$ (732.38): C, 62.32; H, 4.40; N, 11.48; S, 8.76. Found: C, 61.93; H, 3.91; N, 11.50; S, 6.73. UV−Vis (5% $CHCl_3$): λ_{max}, nm (ε, $dm^3mol^{-1}cm^{-1}$) 267 (40300), 298 (30000), 604 (147). FT-IR (KBR): ν, cm^{-1} 3394 (N–H), 1594 (C=O), 1560 (C=N). EPR (300 K): ‘g’ values 2.286, 2.047. EPR (LNT): ‘g’ values 2.220, 2.038.

View Article Online
DOI: 10.1039/C4RA01459F

4.3.2. Bis(*N,N′*-diphenyl-*N″*-thiophenecarbonylguanidinato)copper(II) (2)

Yield: 85%. Light blue solid. M.p.: 215 °C. Anal. Calcd. for $C_{36}H_{28}CuN_6O_2S_2$ (704.32): C, 61.39; H, 4.01; N, 11.93; S, 9.1. Found: C, 61.17; H, 3.45; N, 12.10; S, 8.61. UV−Vis (5% $CHCl_3$): λ_{max}, nm (ε, $dm^3mol^{-1}cm^{-1}$) 269 (14500), 306 (25600), 601 (88). FT-IR (KBR): ν, cm^{-1} 3402 (N–H), 1593 (C=O), 1556 (C=N). EPR (300 K, 'g' value): 2.385, 2.047 EPR (LNT, 'g' value): 2.223, 2.046

4.3.3. Bis(*N*-phenyl -*N′*-benzyl-*N″*-thiophenecarbonylguanidinato)copper(II) (3)

Yield: 83%. Blue solid. M.p.: 202 °C; Anal. Calcd. for $C_{38}H_{32}CuN_6O_2S_2$ (732.38): C, 62.32; H, 4.40; N, 11.48; S, 8.76. Found: C, 62.66; H, 3.72; N, 11.80; S, 7.97. UV−Vis (5% $CHCl_3$): λ_{max}, nm (ε, $dm^3mol^{-1}cm^{-1}$) 254 (13100), 298 (29000), 603 (154). FT-IR (KBR): ν, cm^{-1} 3421 (N–H), 1557 (C=O), 1533 (C=N). EPR (300 K, 'g' value): 2.204, 2.043 EPR (LNT, 'g' value): 2.217, 2.042

4.3.4. Bis(*N*-phenyl -*N′*-butyl-*N″*-thiophenecarbonylguanidinato)copper(II) (4)

Yield: 71%. Light blue solid. M.p: 172 °C. Anal. Calcd. for $C_{32}H_{36}CuN_6O_2S_2$ (664.34): C, 57.85; H, 5.46; N, 12.65; S, 9.65. Found: C, 57.50; H, 5.44; N, 12.48; S, 9.88. UV−Vis (5% $CHCl_3$): λ_{max}, nm (ε, $dm^3mol^{-1}cm^{-1}$) 254 (12900), 298 (28900), 626 (298). FT-IR (KBR): ν, cm^{-1} 3418 (N–H), 1560 (C=O), 1537 (C=N). EPR (300 K, 'g' value): 2.203, 2.022 EPR (LNT, 'g' value): 2.218, 2.042

4.3.5. Bis(*N*-phenyl -*N′*-cyclohexyl-*N″*-thiophenecarbonylguanidinato)copper(II) (5)

Yield: 73%; Light blue solid. M.p.: 210 °C. Anal. Calcd. for $C_{36}H_{40}CuN_6O_2S_2$ (716.42): C, 60.35; H, 5.63; N, 11.73; S, 8.95; Found: C, 59.91; H, 5.05; N, 11.69; S, 8.63. UV−Vis (5% $CHCl_3$): λ_{max}, nm (ε, $dm^3mol^{-1}cm^{-1}$) 254 (4600), 299 (16600), 608 (66). FT-IR (KBR): ν, cm^{-1} 3418 (N–H), 1566 (C=O), 1532 (C=N). EPR (300 K, 'g' value): 2.283, 2.047 EPR (LNT, 'g' value): 2.217, 2.049

4.4. Single crystal X-ray diffraction studies

A Bruker APEX2 X-ray (three-circle) diffractometer was employed for crystal screening, unit cell determination, and data collection. The X-ray radiation employed was generated from a Mo sealed X-ray tube (K_α = 0.70173 Å with a potential of 40 kV, 40 mA) fitted with a graphite monochromator in the parallel mode (175 mm collimator with 0.5 mm

View Article Online
DOI: 10.1039/C4RA01459F

pinholes). Sixty data frames were taken at widths of 0.5°. These reflections were used in the auto-indexing procedure to determine the unit cell. A suitable cell was found and refined by nonlinear least squares and Bravais lattice procedures. The unit cell was verified by examination of the *h k l* overlays on several frames of data by comparing with both the orientation matrices. No super-cell or erroneous reflections were observed. After careful examination of the unit cell, a standard data collection procedure was initiated using omega scans. Integrated intensity information for each reflection was obtained by reduction of the data frames with the program APEX2.[49] The integration method employed a three dimensional profiling algorithm and all data were corrected for Lorentz and polarization factors, as well as for crystal decay effects. Finally, the data were merged and scaled to produce a suitable data set. The absorption correction program SADABS[50] was employed to correct the data for absorption effects. Systematic reflection conditions and statistical tests of the data suggested the space group. Solution was obtained readily using SHELXTL (XS).[51] Hydrogen atoms were placed in idealized positions and were set riding on the respective parent atoms. All non-hydrogen atoms were refined with anisotropic thermal parameters. The structure was refined (weighted least squares refinement on F^2) to convergence.[51, 52] Olex2 was employed for the final data presentation and structure plots.[52]

4.5. DNA binding studies

The interaction of metal complexes with CT DNA was carried out in Tris HCl/NaCl buffer (pH 7.2). The bulk solution of CT DNA was prepared by diluting the CT DNA using Tris HCl/NaCl buffer followed by stirring at 4 °C for three days, and kept at 4 °C for not more than a week. The stock solution of CT DNA gave a ratio of UV absorbance at 260 and 280 nm (A260/A280) of 1.89, indicating that the DNA was sufficiently free of proteins. The bulk DNA solution was further diluted to 10 folds to show maximum absorbance at 260 nm. The absorption coefficient of CT DNA was 6600 cm^{-1} M^{-1} per nucleotide.[53] Cu(II) complexes of required concentration were prepared by dissolving the calculated amount of the complexes in 5% DMF/Tris HCl/NaCl. Complex solution of concentration 15 μM was taken in cuvette and CT DNA of equivalent concentration (5–40 μM) was added each time and the significant absorbance change was noted.

The competitive binding of each complex with EB has been investigated by fluorescence spectroscopic technique in order to examine whether the complex can displace EB from its CT DNA-EB complex. Ethidium bromide solution was prepared using Tris HCl/NaCl buffer (pH 7.2). The test solution was added in aliquots of 2.5 μM concentration to

View Article Online
DOI: 10.1039/C4RA01459F

DNA-EB and the change in fluorescence intensities at 596 nm (450 nm excitation) was noted down.

4.6 Protein binding studies

The binding of copper(II) complexes (**1**-**5**) with BSA was studied using fluorescence spectra recorded at a fixed excitation wavelength corresponding to BSA at 280 nm and monitoring the emission at 335 nm. The excitation and emission slit widths and scan rates were constantly maintained for all the experiments. Stock solution of BSA was prepared in 50 mM phosphate buffer (pH = 7.2) and stored in the dark at 4 °C for further use. Concentrated stock solutions of each test compound were prepared by dissolving them in DMF–phosphate buffer (5:95) and diluted with phosphate buffer to get required concentrations. 2.5 ml of BSA solution was titrated by successive additions of a 10^{-6} M stock solution of the complexes using a micropipette. For synchronous fluorescence spectra measurements, the same concentration of BSA and the complexes were used and the spectra were measured at two different Δλ (difference between the excitation and emission wavelengths of BSA) values of 15 and 60 nm.

4.7. Cytotoxic studies

Cytotoxicity studies of the copper complexes were carried out on human breast (MCF7) and lung (A549) cancer cell lines. Cell viability was carried out using the MTT assay method.[54] The non-small lung adenocarcinoma cells (A549 cells) and human breast cancer cells (MCF-7) were plated separately in 96 well plates at a concentration of 1×10^5 cells/well. Complexes (**1**-**5**) of concentration ranging from 10-200 μM dissolved in DMSO were seeded to the wells. DMSO was used as the control. It is important to mention here that complexes (**1**-**5**) are stable in DMSO. After 24 h, the wells were treated with 20 μL MTT [5 mg/ml phosphate buffered saline (PBS)] and incubated at 37 °C for 4 h. The purple formazan crystals formed were dissolved in 200 μL DMSO. The absorbance of the solution was measured at a wavelength of 570 nm using a Beckmann Coulter Elisa plate. Triplicate samples were analyzed for each experiment. The percentage inhibition was calculated using the formula.

$$\frac{\text{Mean OD of the untreated cells (control)} - \text{Mean OD of the treated cells}}{\text{Mean OD of the untreated cells (control)}} \times 100$$

View Article Online
DOI: 10.1039/C4RA01459F

Acknowledgements

K. J. thanks DST for fellowship under DST INSPIRE programme. We thank Sophisticated Analytical Instrumentation facility (SAIF), Indian Institute of Technology - Madras and Indian Institute of Technology - Bombay for NMR and EPR analyses respectively. R. K. gratefully acknowledges DST for the financial support under FIST programme.

View Article Online
DOI: 10.1039/C4RA01459F

References

1 Y. B. Zeng, N. Yang, W. S. Liu and N. Tang, *J. Inorg. Biochem*., 2003, **97**, 258-264.

2 R. Nagane, T. Koshigoe and M. Chikira, *J. Inorg. Biochem*., 2003, **93**, 204-212.

3 A. Silvestri, G. Barone, G. Ruisi, M. Giudice, S. Tumminello, *J. Inorg. Biochem*., 2004, **98**, 589-594.

4 A. T. Chaviara, P. C. Christidis, A. Papageorgiou, E. Chrysogelou, D. J. Hadjipavlou-Litina and C. A. Bolos, *J. Inorg. Biochem*., 2005, **99**, 2102-2109.

5 T. Fujimori, S. Yamada, H. Yasui, H. Sakurai, Y. In and T. J. Ishida, *J. Biol. Inorg. Chem*., 2005, **10**, 831-841.

6 F. L. Yin, J. Shen, J. J. Zou and R. C. Li, *Acta Chim. Sinica*, 2003, **61**, 556-561.

7 P. M. May, D. R. Williams, *In Metal Ions in Biological Systems*, H. Sigel, Ed., Marcel Dekker, New York, 1981, pp. 283–317.

8 T. Miura, A. Hori-i, H. Mototani and H. Takeuchi, *Biochemistry*, 1999, **38**, 11560–11569.

9 C. Fernandes, G. L. Parrilha, J. A. Lessa, L. J. M. Santiago, M. M. Kanashiro, F. S. Boniolo, A. J. Bortoluzzi, N. V. Vugman, M. H. Herbst and A. Horn Jr, *Inorg. Chim. Acta*., 2006, **359**, 3167–3176.

10 B. C. Bales, T. Kodama, Y. N. Weledji, M. Pitie, B. Meunier and M. M. Greenberg, *Nucl. Acid Res*., 2005, **33**, 5371–5379.

11 P. K. M. Siu, D. L. Ma and C. M. Che, *Chem. Commun*., 2005, 1025-1027.

12 J. N. Tian, J. Q. Liu, X. Tian, Z. D. Hu and X. G. Chen, *J. Mol. Struct*., 2004, **691**, 197-202.

13 J. Seetharamappa and B. P. Kamat, *Chem. Pharm. Bull*., 2004, **52**, 1053-1057.

14 G. Durant, *Chem. Soc. Rev*., 1985, **14**, 375-398.

15 R. G. S. Berlinck, *Nat. Prod. Rep*., 1996, **13**, 377-409.

16 R. G. S. Berlinck, *Nat. Prod. Rep*., 1999, **16**, 339-365.

17 L. Heys, C. G. Moore and P. J. Murphy, *Chem. Soc. Rev*., 2000, **29**, 57-67.

18 P. J. Hajduk, S. Boyd, D. Nettesheim, V. Nienaber, J. Severin, R. Smith, D. Davidson, T. Rockway and S.W. Fesik, *J. Med. Chem*., 2000, **43**, 3862-3866.

19 D. M. Evens, K. Sloanstakleff, M. Arvan and D. P. Guyton, *Clin. Exp. Metastasis*, 1998, **16,** 353-357.

20 J. Chern, Y. Leu, S. Wang, R. Jou, S. Hsu, Y. Liaw and H. Lin, *J. Med. Chem*., 1997, **40**, 2276-2286.

21 Z. Brzozowski, F. Saczewski and M. Gdaniec, *Eur. J. Med. Chem*., 2002, **37**, 285-293.

View Article Online
DOI: 10.1039/C4RA01459F

22 H. Fu, Y. H. Zhou, W. L. Chen, Z. G. Deqing, M. L. Tong, L. N. Ji and Z. W. Mao, *J. Am. Chem. Soc*., 2006, **128**, 4924-4925.

23 M. J. Belousoff, L. Tjioe, B. Graham and L. Spiccia, *Inorg. Chem*. 2008, **47**, 8641-8651.

24 G. Murtaza, A. Badshah, M. Said, H. Khan, A. Khan, S. Khan, S. Siddiq, M. I. Choudhary, J. Boudreauc and F.G. Fontainec, *Dalton Trans*., 2011, **40**, 9202-9211.

25 S. Cunha, M. T. Rodrigues, C. C. de Silva, H. B. Napolitano, I. Vencato and C. Laricci, *Tetrahedron*, 2005, **61**, 10536-10540.

26 S. S. Batsanov, *J. Mol. Struct*., 2011, **990**, 63-66.

27 B. Cordero, V. Gomez, A. E. Platero-Prats, M. Reves, J. Echeverria, E. Cremades, F. Barragan, S. Alvarez, *Dalton Trans*., 2008, 2832-2838.

28 U. Schroder, L. Beyer, R. Richter, J. Angulo-Cornejo, M. Castillo-Montoya and M. Lino-Pacheco, *Inorg. Chim. Acta*, 2003, **353**, 59-67.

29 L. Beyer, R. Richter, R. Wolf, J. Zaumseil, M. Lino-Pacheco and J. Angulo-Cornejo, *Inorg. Chem. Commun.*, 1999, **2**, 184-187.

30 M. J. Begley, P. Hubberstey and C. H. M. Moore, *J. Chem. Res., Synop.*, 1986, **5**, 172-173.

31 A. Tomas, B. Viossat, M. F. Charlot, J. J. Girerd and D. N. Huy, *Inorg. Chim. Acta*, 2005, **358**, 3253-3258.

32 J. S. Guerrero, P. C. Sanchez, E. R. Perez, F. V. Garcia, M. E. B. Gomez and L. R. Azuara, *Toxicology in Vitro, 2011*, **25**, 1376-1384.

33 A. M. Pyle, J. P. Rehmann, R. Meshoyrer, C. V. Kumar, N. J. Turro and J. K. Barton, *J. Am. Chem. Soc*., 1989, **111**, 3051-3058.

34 A. Wolf and G. H. Shimer, T. Meehan, *Biochemistry*, 1987, **26**, 6392-6396.

35 N. Chitrapriya, T. Sathiya Kamatchi, M. Zeller, H. Lee, K. Natarajan, *Spectrochim. Acta Part A*, 2011, **81**, 128-134.

36 J. R. Lakowicz and G. Webber, *Biochemistry*, 1973, **12**, 4161-4170.

37 B. C. Baguley and M. Lebret, *Biochemistry*, 1984, **23**, 937-943.

38 W. D. Wilson, L. Ratmeyer, M. Zhao, L. Strekowski and D. Boykin, *Biochemistry*, 1993, **32**, 4098-4104.

39 K. S. Ghosh, B. K. Sahoo, D. Jana and S. Dasgupta, *J. Inorg. Biochem*., 2008, **102**, 1711-1718.

40 D. Senthil Raja, N. S. P. Bhuvanesh, K. Natarajan, *Eur. J. Med. Chem*., 2011, **46**, 4584-4594.

41 D. Senthil Raja, G. Paramaguru, N. S. P. Bhuvanesh, J. H. Reibenspies, R. Renganathan,

View Article Online
DOI: 10.1039/C4RA01459F

K. Natarajan, *Dalton Trans*., 2011, **40**, 4548-4559.

42 J. R. Lakowicz*, Fluorescence Quenching: Theory and Applications. Principles of Fluorescence Spectroscopy*, Kluwer Academic/Plenum Publishers, New York, 1999, 53-127.

43 X. Z. Feng, Z. Yang, L. J. Wang, C. Bai, *Talanta*, 1998, **47**, 1223-1229.

44 G. Z. Chen, X. Z. Huang, Z. Z. Zheng, J. G. Xu, Z. B. Wang, *Analysis Method of Fluorescence*, 3rd Edition, Science Press, Beijing, 1990.

45 J. N. Miller, *Proc. Anal. Div. Chem. Soc*. 1979, **16**, 203-208.

46 P. Krishnamoorthy, P. Sathyadevi, A. H. Cowley, R. R. Butorac and N. Dharmaraj, *Eur. J. Med. Chem*., 2011, **46**, 3376-3387.

47 T. K. Goswami, B. V. Chakravarthi, M. Roy, A. A. Karande, A. R. Chakravarty, *Inorg. Chem*., 2011, **50**, 8452-8464.

48 S. Cunha, M. B. Costa, H. B. Napolitano, C. Lauriucci, I. Vecanto, *Tetrahedron*, 2001, **57**, 1671-1675.

49 APEX2 "*Program for Data Collection on Area Detectors*" BRUKER AXS Inc., 5465 East Cheryl Parkway, Madison, WI 53711-5373, USA.

50 SADABS, G. M. Sheldrick, "*Program for Absorption Correction of Area Detector Frames*", BRUKER AXS Inc., 5465 East Cheryl Parkway, Madison, WI 53711-5373, USA.

51 G. M. Sheldrick, *Acta Cryst*., 2008, **A64**, 112-122.

52 O. V. Dolomanov, L. J. Bourhis, R. J. Gildea, J. A. K. Howard, H. Puschmann, *J. Appl. Cryst*., 2009, **42**, 339-341.

53 M. E. Reichmann, S. A. Rice, P. Thomas, *J. Am. Chem. Soc*., 1954, **76**, 3047-3053.

54 T. Mossman, *J. Immunol. Methods*, 1983, **65**, 55–63.

View Article Online
DOI: 10.1039/C4RA01459F

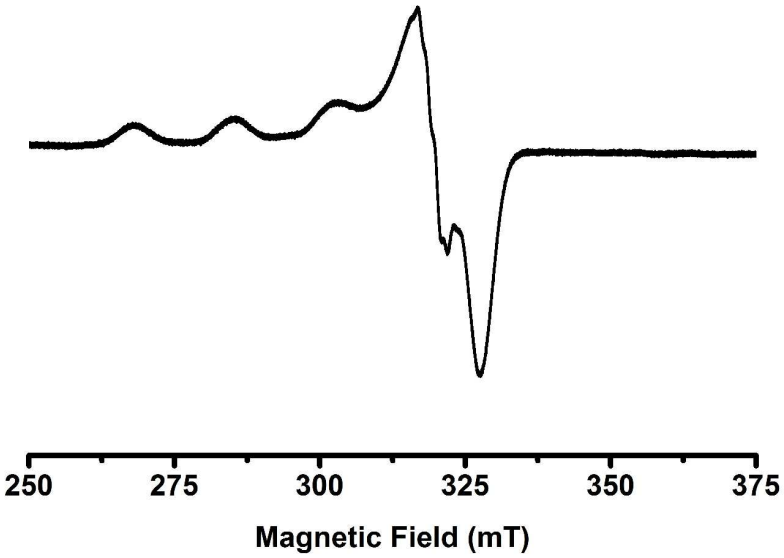

Fig. 1 EPR spectrum of complex **1** in frozen DMF solution. Microwave power, 0.98 mW; microwave frequency, 9.1 GHz.

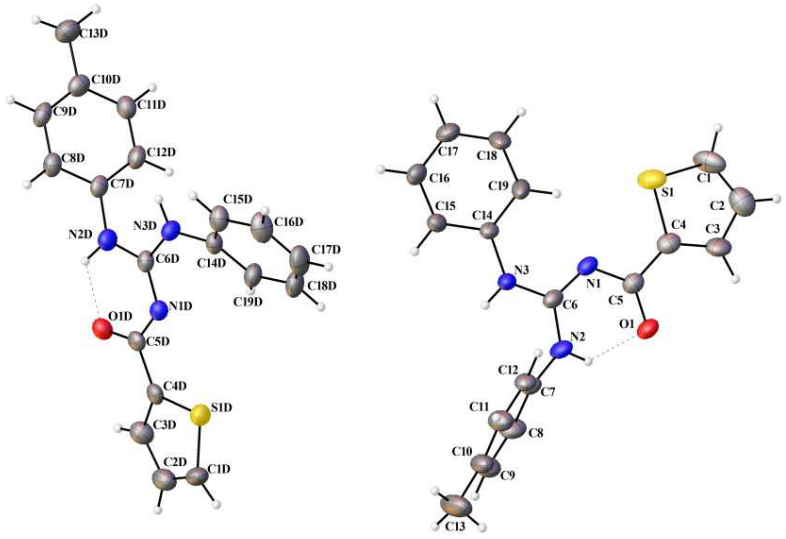

Fig. 2 Thermal ellipsoid plot of L1.

View Article Online
DOI: 10.1039/C4RA01459F

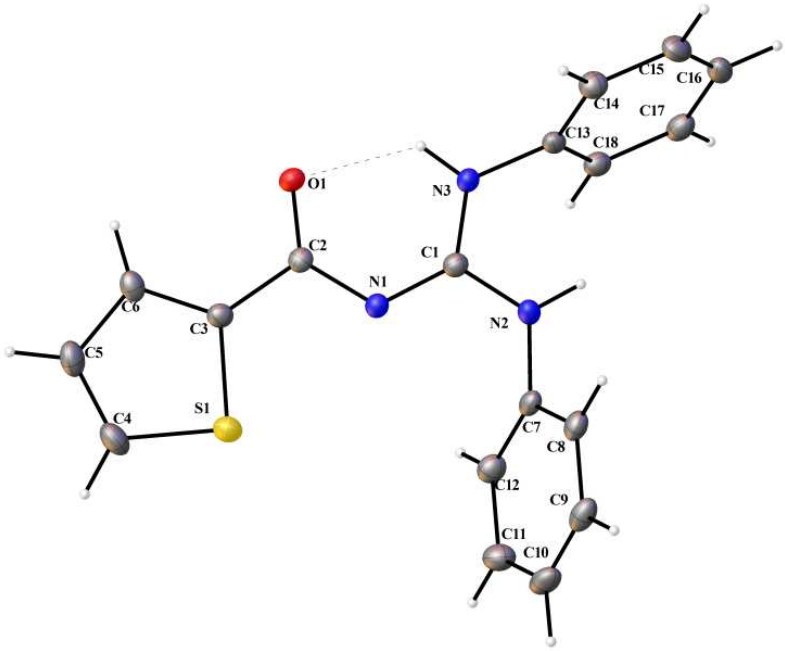

Fig. 3 Thermal ellipsoid plot of L2.

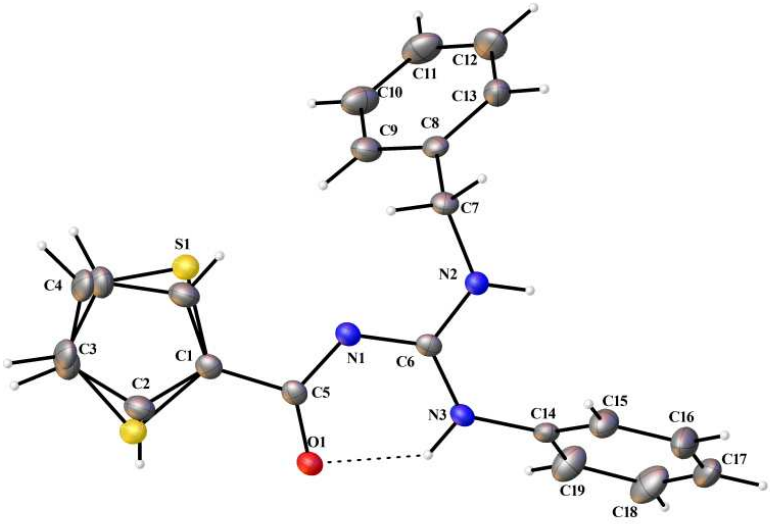

Fig. 4 Thermal ellipsoid plot of L3.

View Article Online
DOI: 10.1039/C4RA01459F

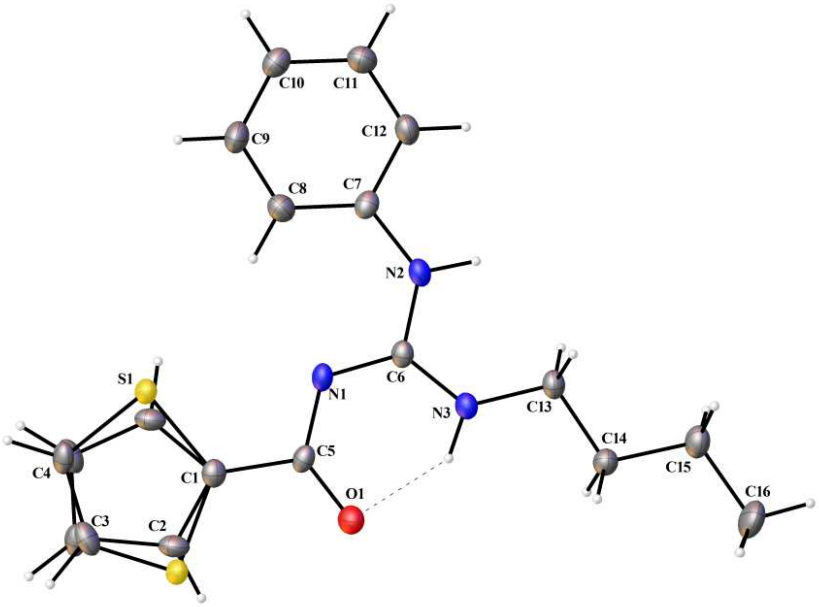

Fig. 5 Thermal ellipsoid plot of L4.

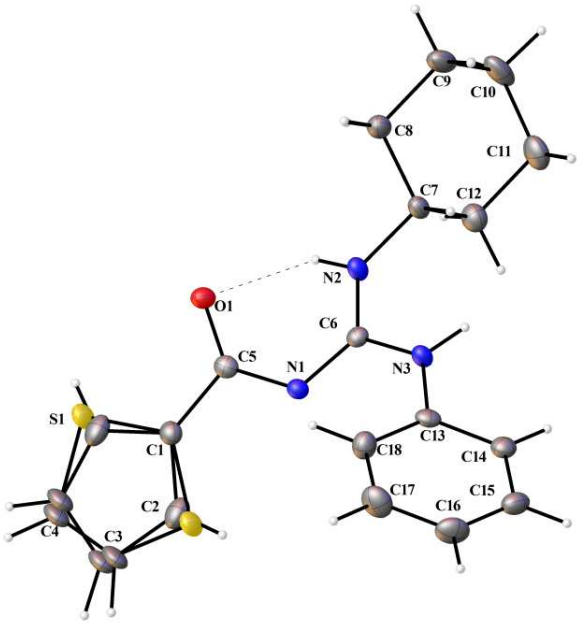

Fig. 6 Thermal ellipsoid plot of L5.

View Article Online
DOI: 10.1039/C4RA01459F

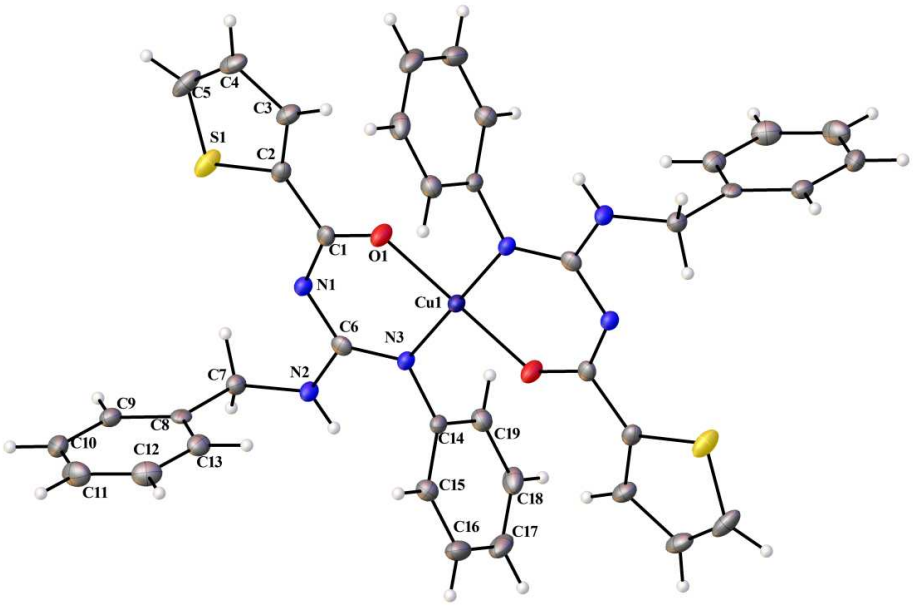

Fig. 7 Thermal ellipsoid plot of **3**.

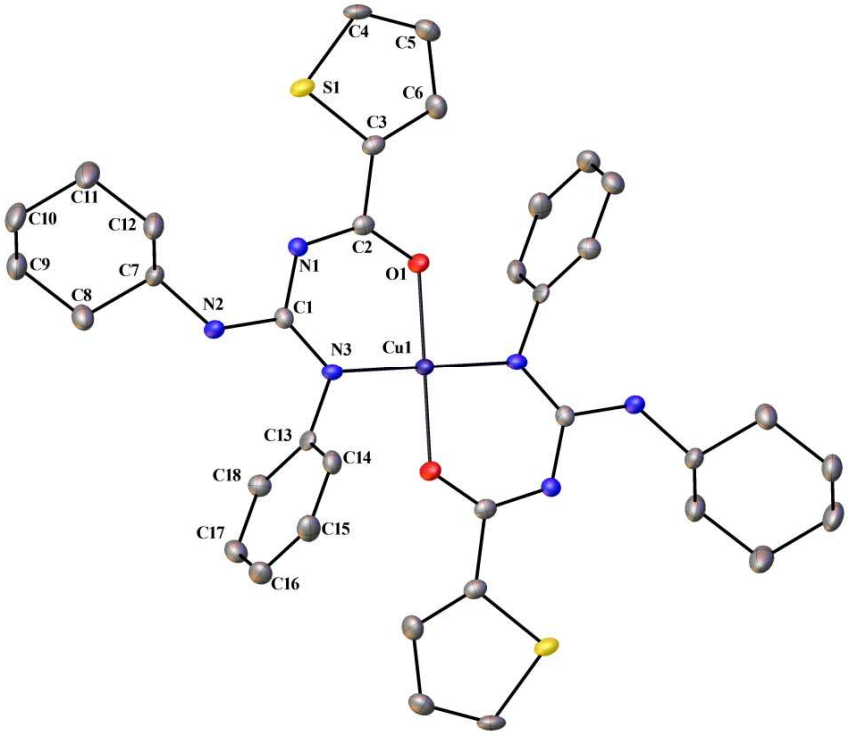

Fig. 8 Thermal ellipsoid plot of **5**.

View Article Online
DOI: 10.1039/C4RA01459F

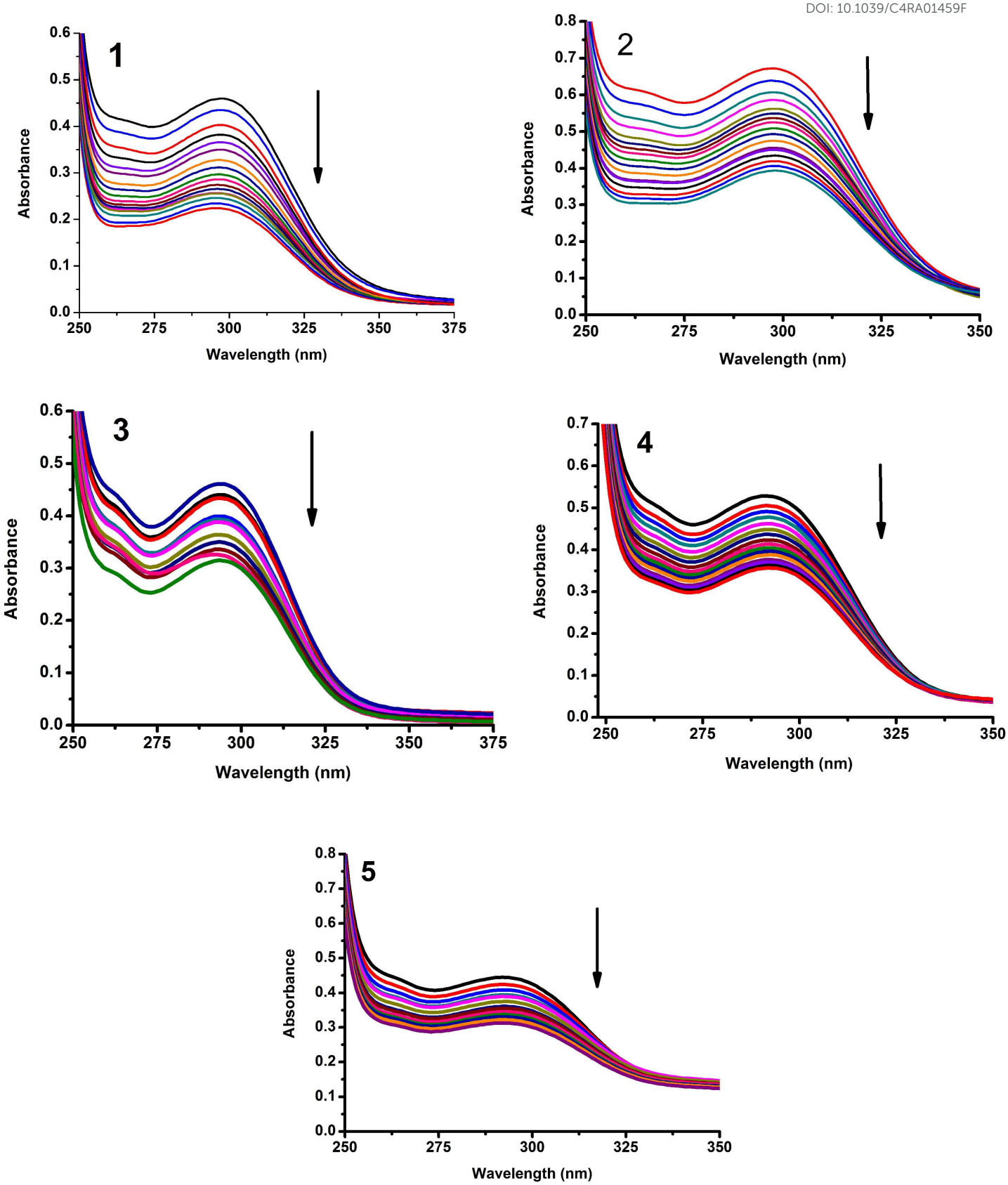

Fig. 9 Absorption spectra of complexes (**1-5**) in Tris-HCl buffer upon addition of CT DNA. [Complex] = 1.5×10^{-5} M, [DNA] = 0-40 μM. Arrow shows that the absorption intensities decrease upon increasing DNA concentration.

View Article Online
DOI: 10.1039/C4RA01459F

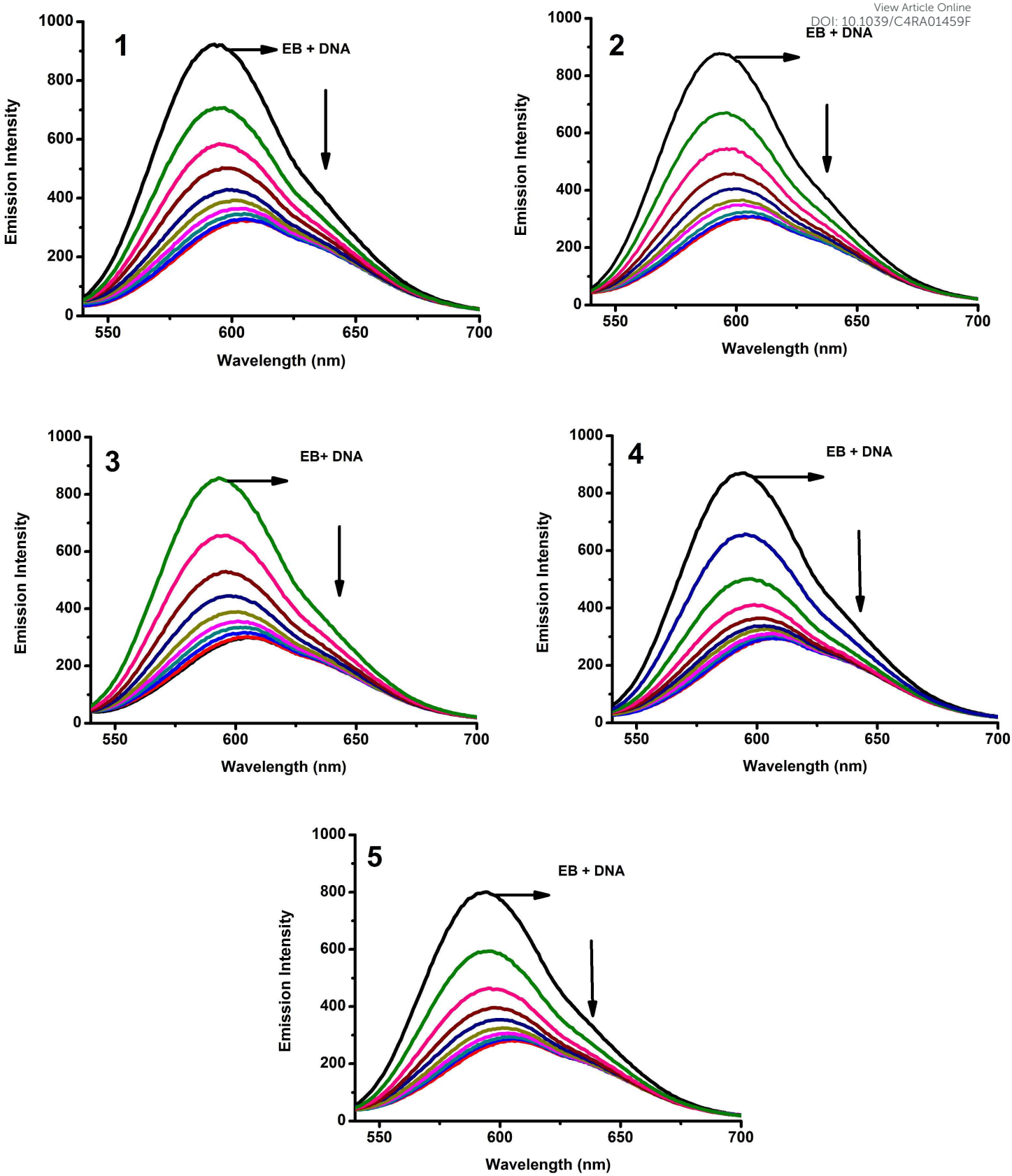

Fig. 10 Fluorescence quenching curves of EB bound to DNA in the presence of **1**-**5**. [DNA] = 5 μM, [EB] = 5 μM and [complex] = 0-25 μM.

View Article Online
DOI: 10.1039/C4RA01459F

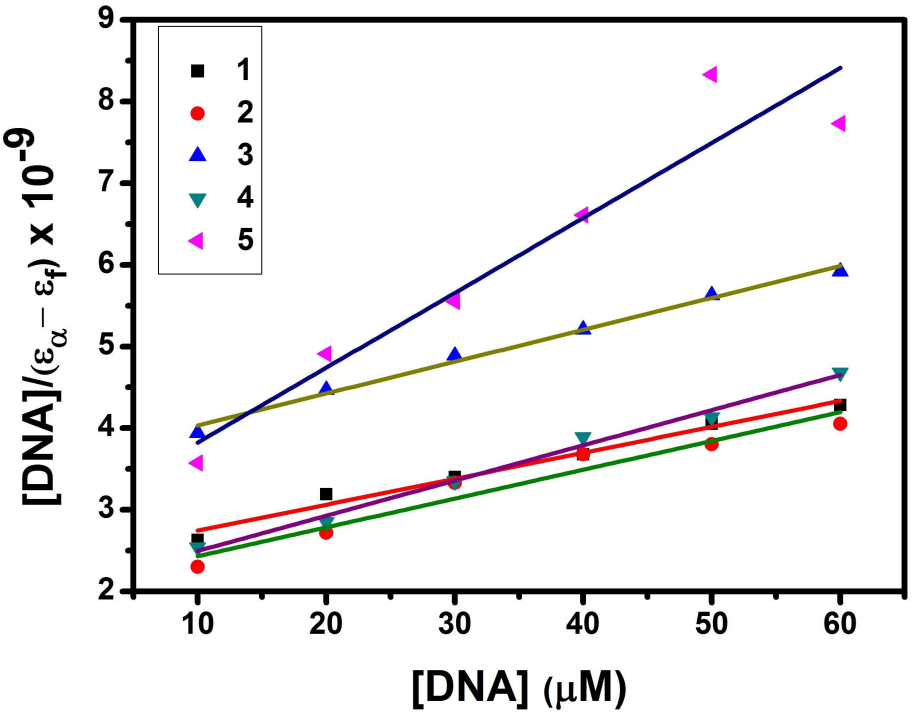

Fig. 11 Plot of [DNA]/($\varepsilon_a - \varepsilon_f$) *versus* [DNA] for the titration of the complexes with CT DNA.

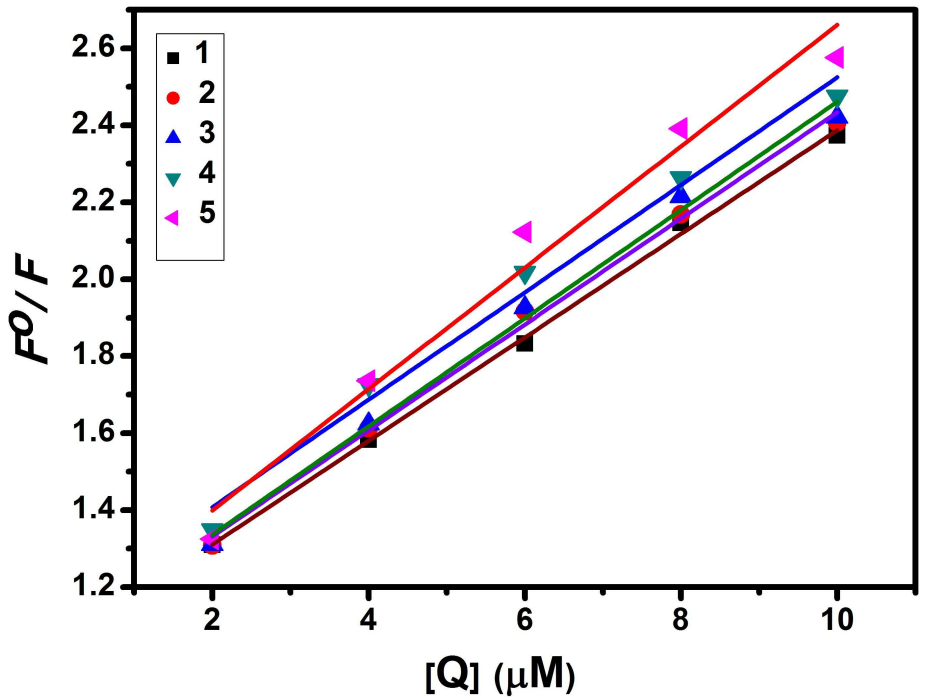

Fig. 12 Stern-Volmer plot of fluorescence titrations of the complexes with CT DNA.

View Article Online
DOI: 10.1039/C4RA01459F

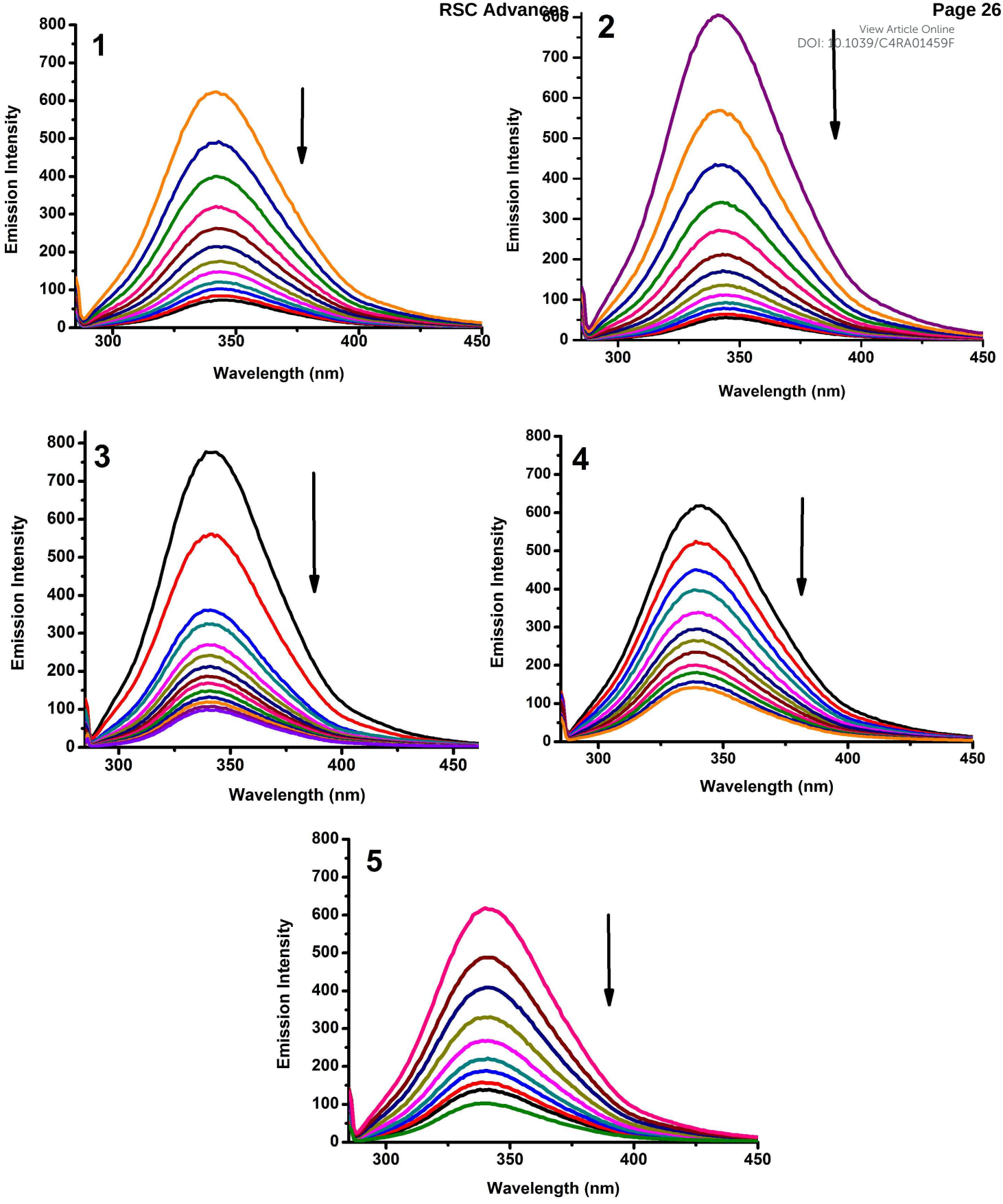

Fig.13 Fluorescence quenching curves of BSA in the absence and presence of **1**-**5**. [BSA] = 1 μM and [complex] = 0-50 μM.

View Article Online
DOI: 10.1039/C4RA01459F

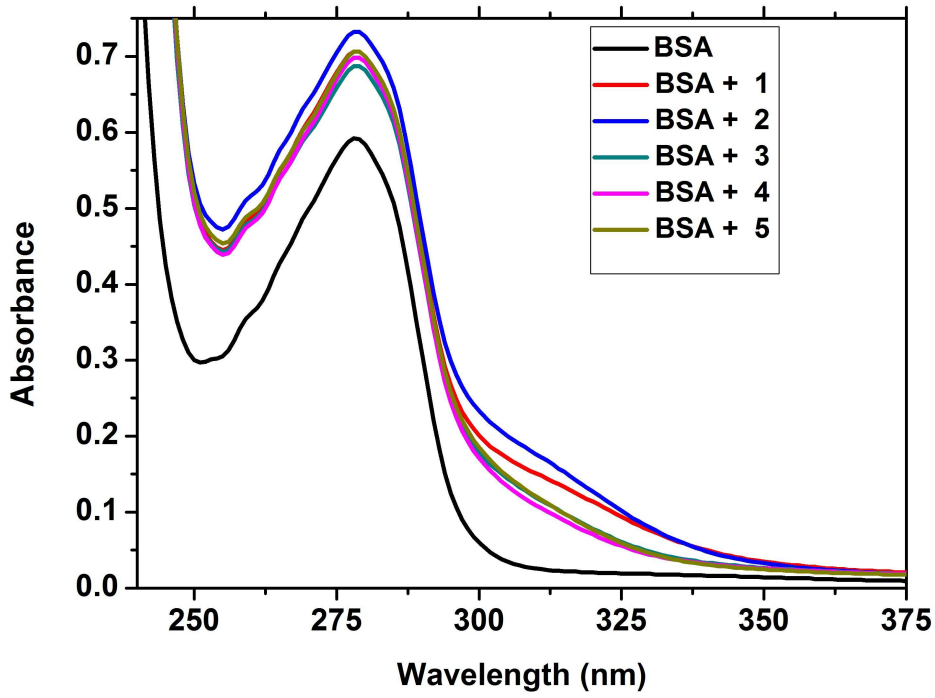

Fig. 14 The absorption spectra of BSA (10 μM) and BSA with **1-5** (4 μM).

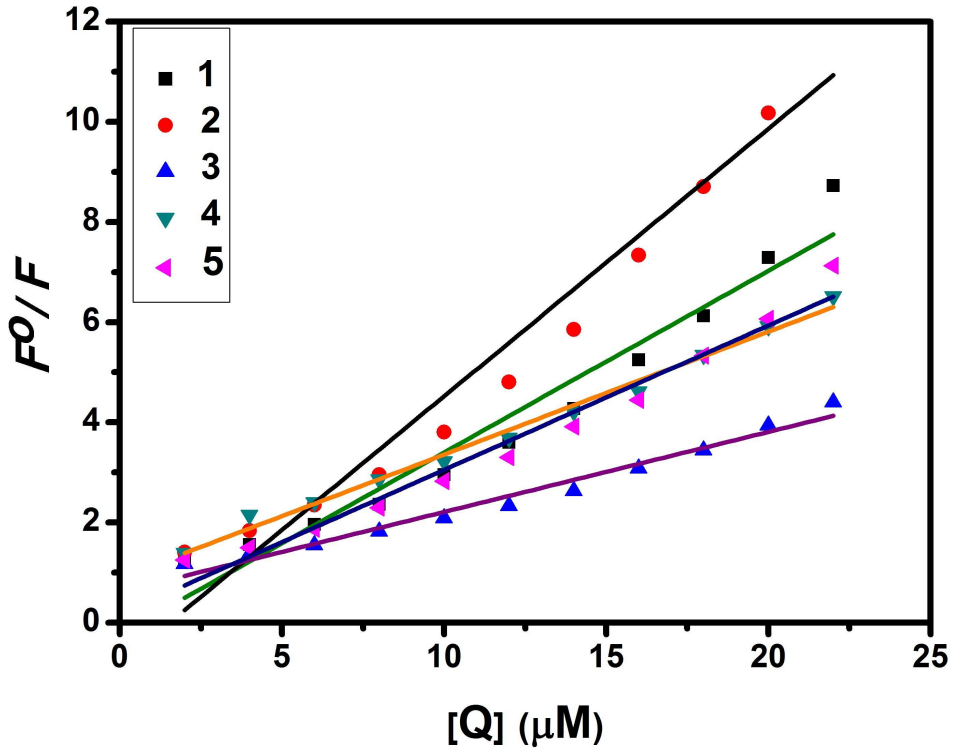

Fig. 15 Stern-Volmer plot of the fluorescence titrations of the complexes with BSA.

View Article Online
DOI: 10.1039/C4RA01459F

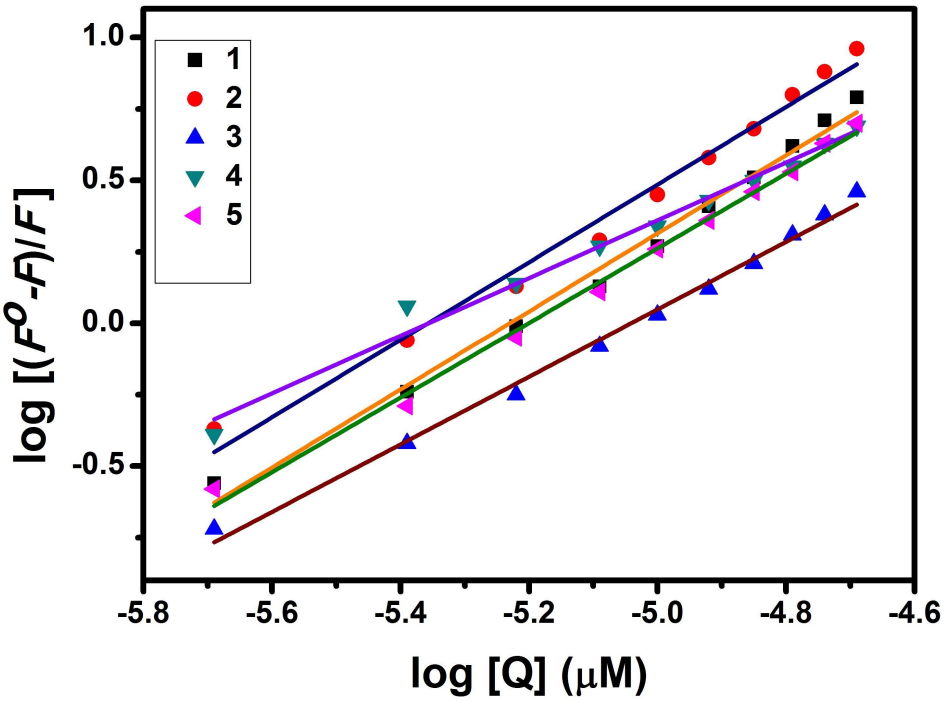

Fig. 16 Scatchard plot of the fluorescence titrations of the complexes with BSA.

View Article Online
DOI: 10.1039/C4RA01459F

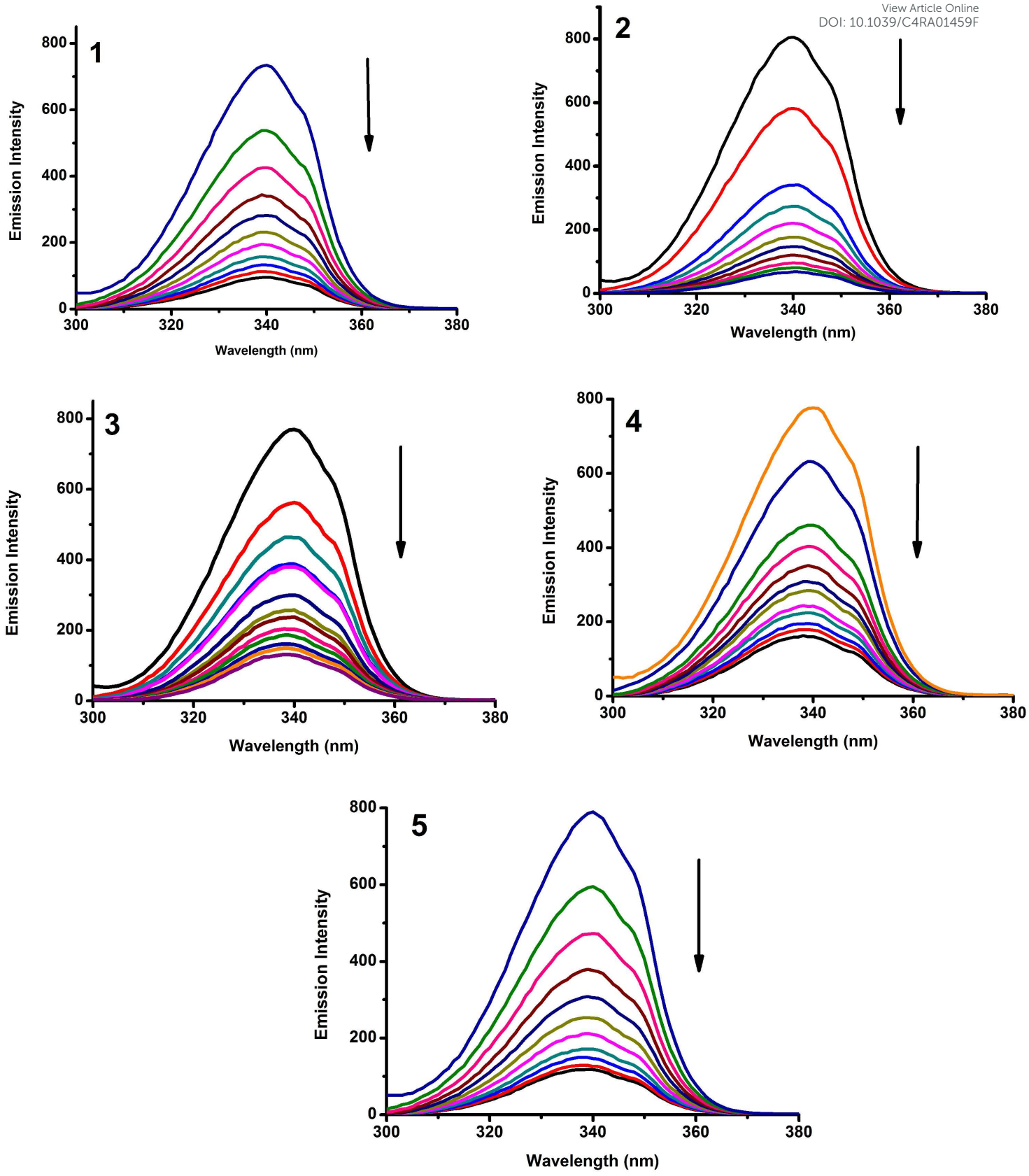

Fig. 17 Synchronous spectra of BSA (1 μM) as a function of concentration of **1-5** (0-50 μM) with $\Delta\lambda$ = 60 nm.

View Article Online
DOI: 10.1039/C4RA01459F

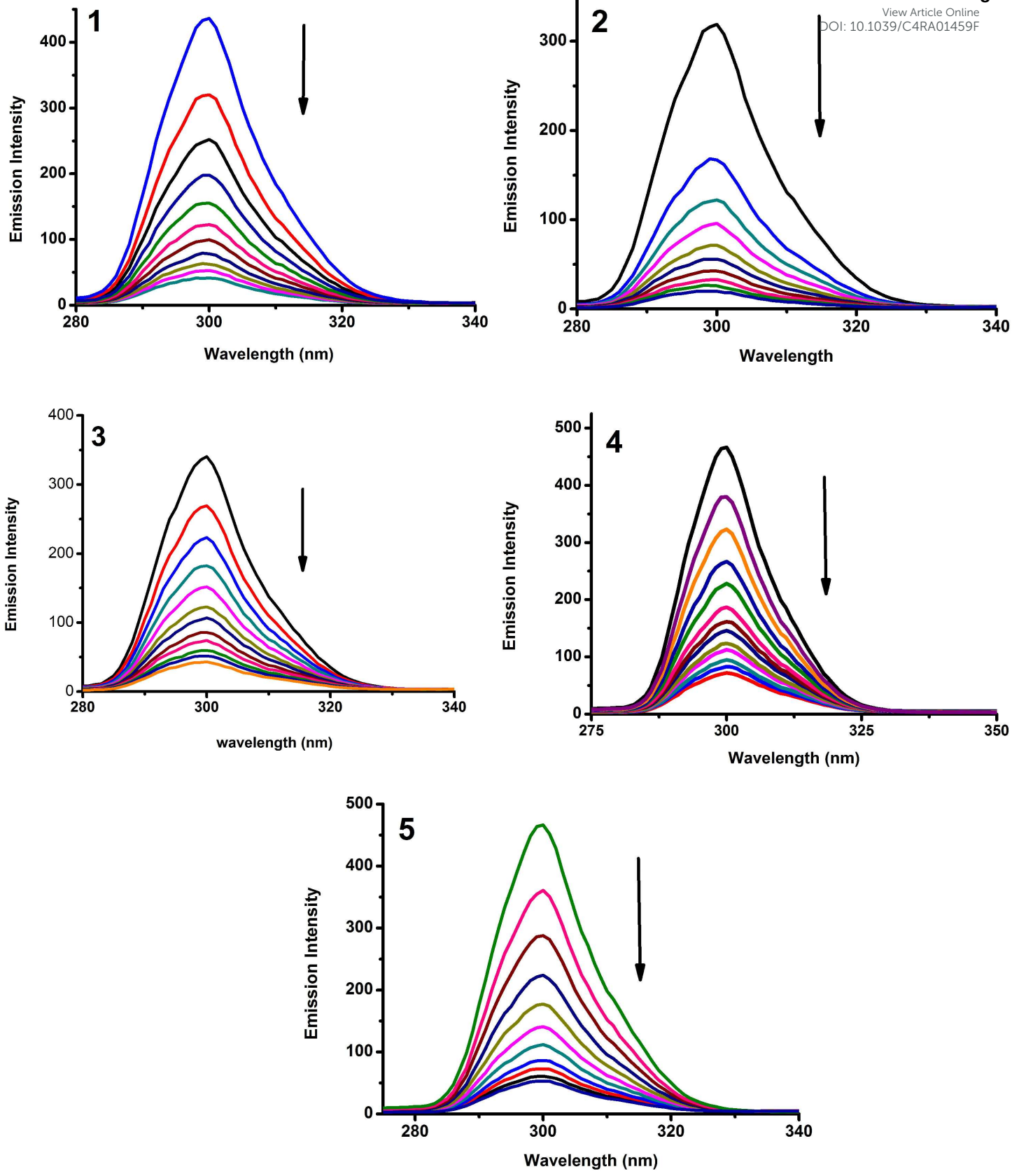

Fig. 18 Synchronous spectra of BSA (1 μM) as a function of concentration of **1-5** (0-50 μM) with $\Delta\lambda$ = 15 nm.

View Article Online
DOI: 10.1039/C4RA01459F

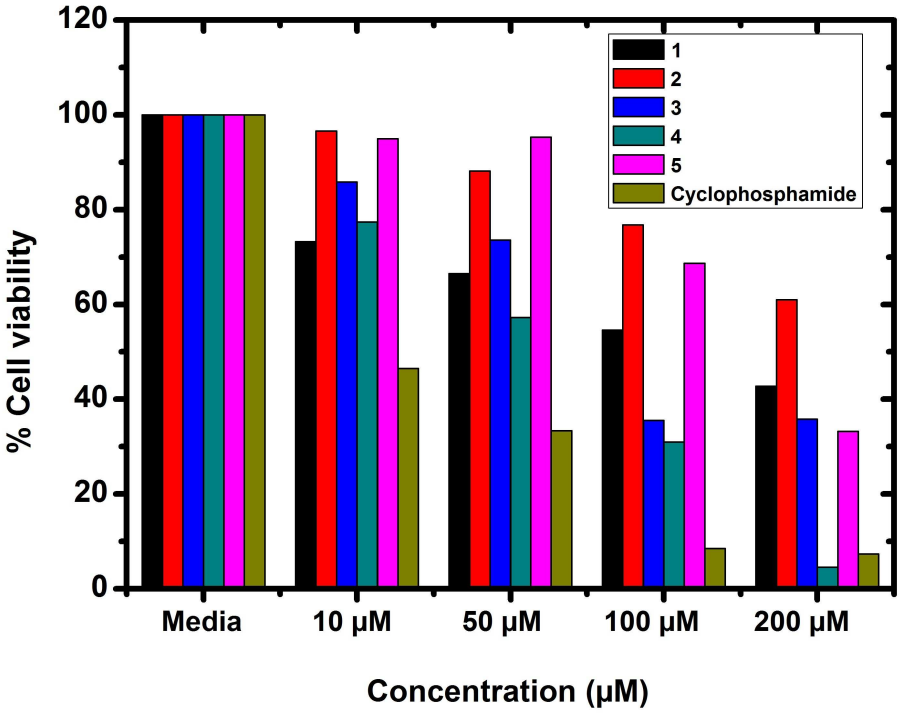

Fig. 19 Cytotoxicity of complexes **1-5** after 24 h incubation on MCF7 cell lines.

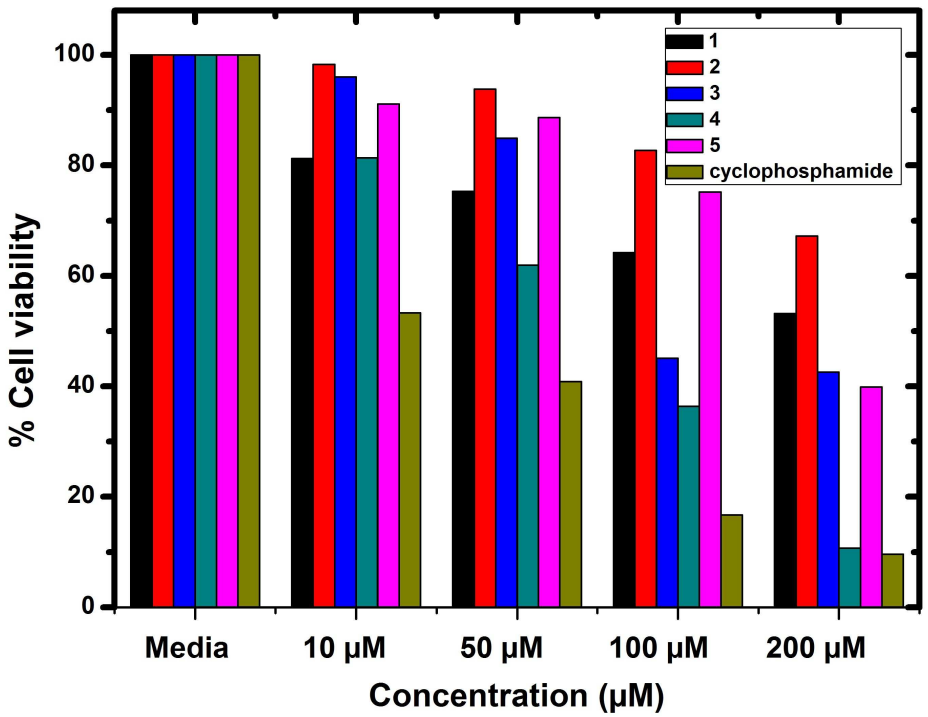

Fig. 20 Cytotoxicity of complexes **1-5** after 24 h incubation on A549 cell lines.

View Article Online
DOI: 10.1039/C4RA01459F

Table 1 EPR parameters of Cu(II) complexes

Complex	Medium & Temp.	$g_{\|}$	g□	$A_{\|}$(G)
1	Solid state RT	2.286	2.047	
	Solution state LNT	2.220	2.038	172
2	Solid state RT	2.385	2.047	
	Solution state LNT	2.223	2.046	173
3	Solid state RT	2.204	2.043	
	Solution state LNT	2.217	2.042	174
4	Solid state RT	2.203	2.022	
	Solution state LNT	2.218	2.042	180
5	Solid state RT	2.283	2.047	
	Solution state LNT	2.217	2.049	181

Table 2 Crystal data and structure refinement for ligands (L1-L5)

	L1	L2	L3	L4	L5
Empirical formula	$C_{19}H_{17}N_3OS$	$C_{18}H_{15}N_3OS$	$C_{19}H_{17}N_3OS$	$C_{16}H_{19}N_3OS$	$C_{18}H_{21}N_3OS$
Formula weight	335.42	321.39	335.42	301.40	327.44
Temperature (K)	110(2)	110(2)	110(2)	110(2)	110(2)
Wavelength (Å)	0.71073	0.71073	0.71073	0.71073	0.71073
Crystal system	Tetragonal	Triclinic	Monoclinic	Monoclinic	Orthorhombic
Space group	*P*-4	*P*-1	*P*2(1)/*n*	*P*2(1)	*Pna*2(1)
Unit cell dimensions					
a (Å)	19.258(5)	6.4059(9)	17.941(4)	7.9816(19)	11.0663(16)
b (Å)	19.258(5)	10.8648(16)	9.5618(19)	9.606(2)	10.4930(15)
c (Å)	9.374(2)	12.1262(17)	20.779(4)	10.048(2)	14.541(2)
α (°)	90	79.907(2)	90	90	90
β (°)	90	82.063(2)	107.292(2)	94.281(3)	90

View Article Online
DOI: 10.1039/C4RA01459F

γ(°)	90	73.721(2)	90	90	90
Volume (Å^3)	3476.6(14)	794.1(2)	3403.6(12)	768.2(3)	1688.5(4)
Z	8	2	8	2	4
Density (calculated) Mg/m^3	1.282	1.344	1.309	1.303	1.288
Absorption coefficient (mm^{-1})	0.196	0.211 mm^{-1}	0.200	0.213	0.200
F(000)	1408	336	1408	320	696
Crystal size (mm^3)	0.60 × 0.50 × 0.20	0.45 × 0.44 × 0.38	0.42 × 0.37 × 0.27	0.37 × 0.27 × 0.03	0.56 × 0.33 × 0.32
Theta range for data collection (°)	1.06 to 27.50	2.42 to 27.44	2.05 to 25.00	2.03 to 25.00	2.39 to 25.00
Index ranges	-24<=h<=24, -24<=k<=24, -12<=l<=12	-8<=h<=8, -14<=k<=13, -15<=l<=15	-21<=h<=21, -11<=k<=11, -24<=l<=24	-9<=h<=9, -11<=k<=11, -10<=l<=11	-13<=h<=13, -12<=k<=12, -16<=l<=17
Reflections collected	38915	8598	31382	4488	13429
Independent reflections [R(int)]	7889 (0.0327)	3538 (0.0141)	5997 (0.0614)	2641 (0.0568)	2952 (0.0285)
Completeness to theta = 27.50°	99.5 %	97.3 %	99.9 %	99.7 %	99.7 %
Absorption correction	Semi-empirical from equivalents	Semi-empirical from equivalents	Semi-empirical from equivalents	Semi-empirical from equivalents	Semi-empirical from equivalents
Max. and min. transmission	0.9618 and 0.8914	0.9240 and 0.9108	0.9479 and 0.9206	0.9936 and 0.9253	0.9388 and 0.8963
Refinement method	Full-matrix least-squares on F^2	Full-matrix least-squares on F^2	Full-matrix least-squares on F^2	Full-matrix least-squares on F^2	Full-matrix least-squares on F^2
Data / restraints /	7889 / 26 / 467	3538 / 0 / 208	5997 / 20 /	2641 / 11 /	2952 / 13 /

View Article Online
DOI: 10.1039/C4RA01459F

parameters			459	205	215
Goodness-of-fit on F^2	1.092	1.063	1.027	1.024	1.053
Final R indices [I>2sigma(*I*)]	R1 = 0.0403, wR2 = 0.0917	R1 = 0.0354, wR2 = 0.0882	R1 = 0.0357, wR2 = 0.0885	R1 = 0.0553, wR2 = 0.1435	R1 = 0.0250, wR2 = 0.0627
R indices (all data)	R1 = 0.0436, wR2 = 0.0939	R1 = 0.0381, wR2 = 0.0898	R1 = 0.0402, wR2 = 0.0921	R1 = 0.0563, wR2 = 0.1456	R1 = 0.0256, wR2 = 0.0633
Largest diff. peak and hole ($e.Å^{-3}$)	0.232 and -0.262	0.385 and -0.377	0.404 and -0.333	0.481 and -0.405	0.123 and -0.161

Table 3 Crystal data and structure refinement for complexes (**3** and **5**)

	3	**5**
Empirical formula	$C_{38}H_{32}CuN_6O_2S_2$	$C_{36}H_{40}CuN_6O_2S_2$
Formula weight	732.36	716.40
Temperature (K)	110(2)	110(2)
Wavelength (Å)	1.54178	1.54178
Crystal system	Triclinic	Monoclinic
Space group	*P*-1	*C*2/*c*
Unit cell dimensions		
a (Å)	8.8813(5)	32.090(2)
b (Å)	9.9783(6)	6.3662(4)
c (Å)	10.5085(6)	18.8845(13)
α (°)	65.333(4)	90
β (°)	83.253(4)	118.786(4)

View Article Online
DOI: 10.1039/C4RA01459F

γ(°)	86.906(4)	90
Volume (Å^3)	840.41(8)	3381.2(4)
Z	1	4
Density (calculated) Mg/m^3	1.447	1.407
Absorption coefficient (mm^{-1})	2.438	2.404
F(000)	379	1500
Crystal size (mm^3)	0.16 × 0.06 × 0.04	0.12 × 0.07 × 0.05
Theta range for data collection (°)	4.66 to 59.99	5.35 to 60.00°.
Index ranges	-9<=h<=9, -11<=k<=11, -11<=l<=11	-36<=h<=36, -6<=k<=6, -20<=l<=20
Reflections collected	14731	25427
Independent reflections [R(int)]	2447 (0.0467)	2425 (0.0741)
Completeness to theta = 27.50°	97.9 %	96.7 %
Absorption correction	Semi-empirical from equivalents	Semi-empirical from equivalents
Max. and min. transmission	0.9088 and 0.6963	0.8893 and 0.7613
Refinement method	Full-matrix least-squares on F^2	Full-matrix least-squares on F^2
Data / restraints / parameters	2447 / 0 / 224	2425 / 10 / 227
Goodness-of-fit on F^2	1.092	1.089
Final R indices [I>2sigma(*I*)]	R1 = 0.0349, wR2 = 0.0956	R1 = 0.0336, wR2 = 0.0869
R indices (all data)	R1 = 0.0393, wR2 = 0.0973	R1 = 0.0390, wR2 = 0.0887
Largest diff. peak and hole (e.Å^{-3})	0.321 and -0.472	0.304 and -0.521

View Article Online
DOI: 10.1039/C4RA01459F

Table 4 Selected bond lengths (A°), angles (°) of ligands

	L1	L2	L3	L4	L5
O(1)-C(5)	1.254(2)	1.2463(16)	1.2614(18)	1.248(3)	1.2560(16)
N(1)-C(6)	1.334(3)	1.3322(17)	1.3427(19)	1.350(3)	1.3413(17)
N(1)-C(5)	1.354(2)	1.3552(16)	1.3441(19)	1.359(4)	1.3476(17)
N(2)-C(6)	1.339(2)	1.3532(17)	1.3338(19)	1.357(4)	1.3290(18)
N(2)-C(7)	1.426(3)	1.4240(17)	1.4705(19)	1.421(3)	1.4648(17)
N(3)-C(6)	1.355(2)	1.3433(16)	1.3517(19)	1.329(4)	1.3566(18)
N(3)-C(14)	1.413(2)	1.4322(16)	1.4238(19)	1.457(3)	1.4230(18)
N(2)-H(2D)	0.8800	0.8800	0.8800	0.9245	0.8800
N(3)-H(3D)	0.8800	0.8800	0.8800	0.9001	0.8800
S(1)-C(4)	1.728(2)	1.7069(15)	1.719(2)	1.716(4)	1.740(3)
S(1)-C(1)	1.712(4)	1.7201(13)	1.7273(15)	1.725(3)	1.6980(15)
O(1)-C(5)-N(1)	127.87(19)	128.29(12)	127.58(14)	128.9(2)	127.67(12)
C(6)-N(1)-C(5)	119.67(16)	120.08(11)	121.95(13)	119.5(2)	120.34(11)
N(2)-C(6)-N(1)	123.78(18)	117.54(12)	117.22(13)	118.6(3)	123.46(12)
N(2)-C(6)-N(3)	116.68(17)	117.04	119.83(13)	117.2(2)	118.51
N(1)-C(6)-N(3)	119.68(17)	125.41(12)	122.95(13)	124.2(2)	117.99(12)
C(6)-N(3)-C(14)	127.94(17)	123.50(11)	128.06(12)	126.6(2)	126.70(11)
C(6)-N(2)-C(7)	127.82(17)	125.62(11)	122.93(13)	130.6(2)	128.54(11)

Table 5 Selected bond lengths (A°), angles (°) of complexes

	3	**5**
Cu(1)-O(1)	1.9087(16)	1.9069(15)
Cu(1)-O(1)#1	1.9087(16)	1.9070(15)

View Article Online
DOI: 10.1039/C4RA01459F

Cu(1)-N(3)	1.9589(19)	1.9688(18)
Cu(1)-N(3)#1	1.9589(19)	1.9688(18)
O(1)-Cu(1)-N(3)	90.30(7)	90.37(7)
O(1)#1-Cu(1)-N(3)#1	90.29(7)	90.37(7)
O(1)#-Cu(1)-N(3)	89.71(7)	89.63(7)
O(1)-Cu(1)-N(3)#	89.70(7)	89.63(7)
O(1)#-Cu(1)-O(1)	180.00	180.00
N(3)-Cu(1)-N(3)#	180.00(10)	180.00
N(1)-C(6)-N(3)	126.82(2)	126.1(2)
N(1)-C(6)-N(2)	113.2(2)	113.16(19)
N(3)-C(6)-N(2)	120.0(2)	120.6(2)

Symmetry transformations used to generate equivalent atoms: #1 -x,-y,-z

Table 6 DNA binding constant (K_b), Stern-Volmer constant (K_q) and the apparent binding constant (K_{app}) for complexes **1-5**

Complex	K_b (M^{-1})	K_q (M^{-1})	K_{app} (M^{-1})
1	1.30×10^4	1.11×10^5	5.55×10^6
2	1.39×10^4	1.07×10^5	5.35×10^6
3	1.69×10^4	1.14×10^5	5.70×10^6
4	1.20×10^4	1.07×10^5	5.35×10^6
5	2.41×10^4	1.30×10^5	6.50×10^6

Table 7 Protein binding constant (K_b), quenching constant (K_q) and number of binding sites (n) for complexes **1-5**

Complex	K_b (M^{-1})	K_q (M^{-1})	n
1	2.00×10^7	2.31×10^5	1.39
2	2.72×10^7	3.35×10^5	1.38
3	3.18×10^5	1.32×10^5	1.02
4	1.52×10^6	2.20×10^5	1.22
5	8.00×10^6	2.09×10^5	1.32

View Article Online
DOI: 10.1039/C4RA01459F

Table 8 *In vitro* cytotoxic studies of Cu(II) complexes against MCF7 and A549 cancer cell lines

Complex	IC 50	
	MCF7 (μM)	A549 (μM)
1	128.67	241.58
2	300.57	370.21
3	76.05	91.68
4	61.08	68.84
5	145.40	164.01
Cyclophosphamide	6.58	22.36

View Article Online
DOI: 10.1039/C4RA01459F

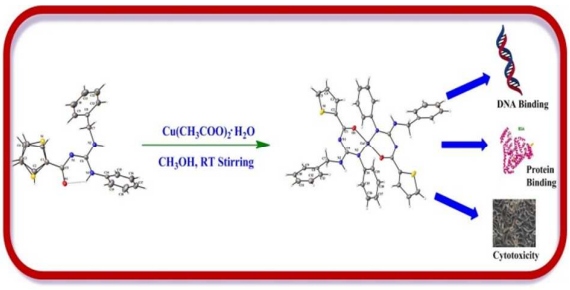

Copper(II) complexes containing *N, N′, N″*-trisubstituted thiophene based guanidine ligands have been synthesized and evaluated for their biological activity.